UNIVERSITY OF NAIROBI

FACULTY OF SCIENCE AND TECHNOLOGY

DEPARTMENT OF PHYSICS

FIRST PRINCIPLES CALCULATIONS OF STRUCTURAL, ELECTRONIC, MECHANICAL, AND OPTICAL PROPERTIES OF TETRA POTASSIUM DIARSENIDO ZINCATE (K_4ZnAs_2) PNICTIDE TERNARY SEMICONDUCTOR.

BY

SAMUEL WAFULA

REG.NO: I56/12499/2018

A Thesis Submitted in Partial Fulfilment of the Requirements for the Degree of Master of Science in Physics at the University of Nairobi.

September, 2023

DECLARATION

I declare that this research work is original and has not been submitted elsewhere for publication. Where other people's work or my own work has been used, this has been properly acknowledged and referenced, in accordance with the University of Nairobi's requirements.

Signature …… Date…7/122023

SAMUEL WAFULA

I56/12499/2018

Department of Physics, University of Nairobi

This thesis is submitted for examination with our approval as a research supervisor.

Signature …… Date 09/12/2023

Prof. Robinson Musembi

Department of Physics

University of Nairobi

P.O Box 30197-00100 Nairobi, Kenya

Email: musembirj@uonbi.ac.ke.

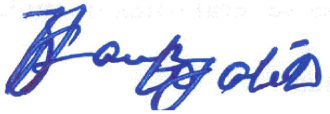

Signature …… Date…9/12/2023…

Prof. Francis Nyongesa

Department of Physics

University of Nairobi

P.O Box 30197-00100 Nairobi, Kenya

Email: fnyongesa@uonbi.ac.ke.

ACKNOWLEDGEMENT

I express my deepest gratitude to my supervisors, Professor Robinson Musembi and Professor Nyongesa, for their guidance and inspiration. Minus them, I wouldn't have a succeeded to complete this work. Personally, I appreciate them because they were approachable and always available for advice. They helped me understand the calculations related to the density functional theory of matter. I would also like to thank my two fellow students, with whom we were mentored by my supervisors, Mr. Martin Nyamunga and Ms. Mauwa Namisi. They always advised me, especially when I did not understand the concept well. Sharing the same student-level discussion board, I was able to understand much in the DFT field. The opportunity to interact with students from the Kaimosi Friends University College also helped me learn more about how to perform DFT calculations using Thermo_pw. This makes my research enjoyable and rewarding. Therefore, I would like also to appreciate the entire family of the Kaimosi University College. In conclusion, I would like to pass my appreciations to everyone who supported me to ensure that this work was successful. Thanks very much. Most of all, I want to thank our Almighty God, who has given us good health to enable us to relate to each other in a healthy way. The glory goes back to Him.

ABSTRACT

The scientific search for materials with good light energy absorption and desirable optical and electrical properties for applications in the areas of optoelectronics like photovoltaic is on the rise globally. Since the optoelectronic potential, intrinsic stability, eco-friendliness and conversion efficiency of most classes of semiconductor materials are not well researched, there is a need for an extensive study to provide an insight and the comprehensive properties of all classes of semiconductor compounds. This motivated us to perform *ab initio* DFT calculations based on plane wave self-consistent field technique for structural, electronic, mechanical, elastic, and optical properties using two exchange correlation functionals: the LDA and the GGA. The one based on LDA was Perdew-Zunger while those based on the GGA were Becke-Lee-Yang-Parr, Engel-Vosko, Perdew-Burke-Ernzerhof, Perdew-Burke-Ernzerhof for solids and Second-order correlations. The bandgap of the material was from the range of 0.5493 eV to 1.2282 eV, suggesting that the band gap is within the visible region. This indicates that the material is suitable for optoelectronic application in photovoltaic. The analysed electronic structure of the projected density of states using the PAW pseudopotentials displayed that the valence band was mainly dominated by As 2p, Zn 2p, Zn 1s, and K 2s, with other orbitals giving a very minimal contributions, whereas the conduction band of the material was mainly dominated by Zn 1s and Zn 2p, with small contributions from As 2p and K 2s orbitals, with the other orbitals making insignificant contributions. The most important and fundamental conditions for the elastic stability of rhombohedra lattice was satisfied. The optical properties displayed the material to have an excellent absorption of light energy within the visible region, which supports the results obtained for the band gap. The average lattice parameter was a = 18.2477, which is comparable with the one in the experimental results indicated in the open literature. The bulk moduli values of the six exchange correlations ranged from 13.3GPa-22.2GPa. The Young Moduli values ranged from 19.1GPa-20.9GPa. The Shear moduli values ranged from 7.4GPa- 7. 8GPa.The poison's ratios ranged from 0.26-0.28. This information suggests that the material is ductile, mechanically stable, ionic, and anisotropic when subjected to external forces.

DEDICATION

I dedicated this work to my fellow students, whom we soldiered together in unravelling the Density Functional Theory DFT calculations and their applications.

TABLE OF CONTENTS

LIST OF TABLES

LIST OF FIGURES

LIST ACRONYMS AND SYMBOLS

AE	All electron wave function
Al	Aluminium
AlInGaP	Aluminium Indium Gallium Phosphide
A	Antimony
As	Arsenic
Bi	Bismuth
BCC	Body Cantered Crystal
B	Boron
BLYP-GGA	Becke- Lee-Young-Parr Generalised Gradient Approximation.
CdS	Cadmium Sulphite
CuAlS2	Copper Aluminum disulphide
CuGaS2	copper gallium Diselenide
CuInSe2	copper indium Diselenide
DFT	Density functional theory
DFT + U	Density functional theory with Hubbard potential
Edc	Energy of particle interactions
EDFT+U	Total energy of density functional theory in coulomb force
E_{XC}^{LDA}	Energy under local density approximation of exchange correlation functions
EV-GGA	Engel Vosko Generalised Gradient Approximation.
n(r)	Electron density
eV	electron volt
FCC	Face cantered cubic
Ga	Gallium
GaAs	Gallium Arsenide
GaN	Gallium nitride
GGA	Generalized gradient approximation
GGA-PBE	Generalized gradient approximation-Perdew Burke Ernzerhof
GGA+U	Generalized gradient approximation with Hubbard potential
Ge	Germanium
GRP	Group
H	Hamiltonian operator
HEG	High extra gas

H-K	Hohenberg-Kohn theorem
In	Indium
InGaAs	Indium Gallium Arsenide
K.E	Kinetic energy
K-S	Kohn Sham Theorem/ equation
KKR	Koringa-Kohn-Rodtoker
LMTO	Linear muffin tin orbital
Ψ	Wave function
Me	Mass of electron
N	Nitrogen
O2	Oxygen
PBE	Perdew-Burke-Ernzerhof
ε	Permittivity
P	Phosphorus
K	Potassium
R.H.S	Right Hand Side
SHG	Second Harmonic Generation
Si	Silicon
SO-GGA	Second Order Generalised Gradient Approximation.
UV	Ultra Violet
TB-MB	Terabyte- Megabyte
K4ZnAs2	TetrapotassiumDiarsenidozincate
Sc	Self consistent
Scf	Self consistent field
SiC	Silicon Carbite
SHG	Second Harmonic Generation
AgInS2	Silver Indium Selenide
K4ZnAs	Tetra potassium Zinc Arsenide
K3As	Tripotasium Arsenide
K3Cu3P2	Tripotasiumtricopperdiphosphide
K3Ni3P2	Tripotasiumtrinickeldiphosphide
Ve-e	electron- electron interaction potential
Veff(r)	Effective potential

Vext	external potential Energy
VH	Hartree potential
Vn-e	nuclear- electron interaction potential
Vn-n	nuclear –nuclear interaction
VXC	Exchange correlation potential
XC	Exchange correlation potential
Zn	Zinc
ZnSiP2	Zinc silicon diphosphate
Outdir	output director,
Pseudo-dir	pseudo potential directory
∇_i^2	laplacian operator of electrons
∇_I^2	laplacian operator of nuclei
QE	Quantum espresso.

CHAPTER ONE: INTRODUCTION

1.0 Introduction

This chapter contains information on semiconductors, with the main focus on the classification of ternary chalcogenides broadly into two categories. Ternary pnictides are discussed from broad to specific; thereafter, the statement of the problem, objectives followed by the significance, and then the justification of the research on the trigonal structure of Zintl phased tetrapotassium diarsenidozincate(K_4ZnAs_2) semiconductor compound based on ab initio molecular studies.

1.1 Background of the Study

Optoelectronic industries are currently competing to produce devices with good energy efficiency and low power consumption, as these are the factors that attract most consumers. This desire has not gone unnoticed within the scientific community, where there has been an increase in scientific research to obtain exemplary semiconductor materials with desirable qualities such as high power efficiency, high temperature stability, turntable band gap, high dielectric constant, and perfect performance for applications in advanced technological fields such as optoelectronics, thermoelectrics, spinotronics, photodetectors, and biomedical imaging. (Mbilo et al., 2022). Semiconductor research began when Group IV elemental semiconductor materials (silicon, Si, germanium, and Ge) were discovered. This was a phase-one evolution in the fields of computing and optoelectronic operations (Berends et al., 2019). The most desirable properties and applications have been achieved using cadmium, cadmium, plumbum, and Pb-based semiconductor compounds. However, for several decades, such materials have encountered opposition in their applications owing to the toxicity of Pb and Cd (Liu *et al*., 2016).

Researchers are now shifting their interest to non-Cd- and Pb-based semiconductor compounds that are non-toxic, cheap, and readily available with high potential for providing high energy to be used for specific applications such as microelectronics, optoelectronics, excellent thermophysical and thermo-electrical materials, nuclear energy production, and magnetic storage materials (Zeb et al., 2020),(Faculty and Fulfilment, 2006).

1.2 Types of Semi-Conductors

Semiconductor materials are broadly classified into two categories: elemental and compound. Elemental semiconductors are the group four elements of an elementary periodic table.

Examples include silicon (Si) and Germanium (Ge). Their structures resemble those of diamond, with an FCC lattice structure having a basis with identical atoms (Idrissi et al., 2021).

Each atom has four neighbouring atomic particles that form a regular tetrahedral structure (RVelavan, and MyvizhiP. 2018). The tetrahedral crystal structures of Si and Ge are shown in Figures 1.1 a and b (Javey, 2006).

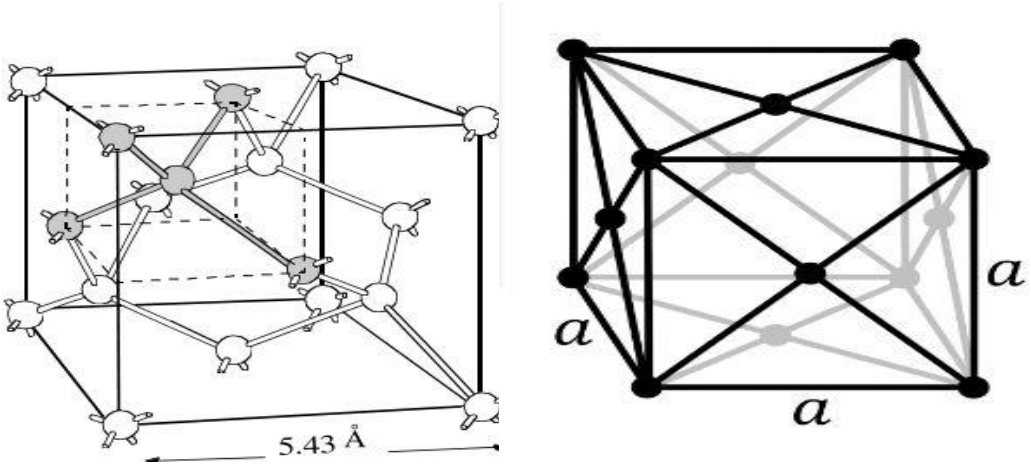

(a) (b)

Figure 1.1: Crystal structures of semi-conductors. (a) Silicon. (b) Cubic structure of Germanium of side a unit (Javey, 2006).

Compound semiconductors contain two or more elements from different groups of elementary periodic tables (Idrissi et al., 2021). These materials typically belong to groups III-V. Examples of group III elements are Indium (In), Gallium (Ga),Boron (B), Aluminium (Al), while group V elements are Nitrogen (N), phosphorus (P), Arsenic (As), Antimony (A) and Bismuth (Bi) (Berends et al.,2019) .Compound semiconductor structures contain elements that can form different complex structures depending on their bonding processes. They can form binary (two elemental structures, e.g. GaAs), ternary structures (three elemental structures: Indium Gallium Arsenide (InGaAs) and Tetra potassium di-arsenido Zicate (K_4ZnAs_2), or even quaternary crystal structures (four elemental structures, for example, Aluminium-Indium Gallium Arsenide (AlInGaP) (Berends et al.,2019).

Compound semiconductor materials have high efficiency performance properties such as high-power yield, modified optical and structural properties, and relatively high frequency compared to elemental semiconductor materials (Idrissi et al., 2021).

These properties provide room for band gap engineering which helps researchers alter the position of the band gap within the material (Berendset et al., 2019).

1.3 Binary and Ternary Semiconductor Materials

1.3.1 Binary Semiconductors

Binary semiconductors have two elements in their crystal structure e.g., Silicon Carbide (SiC), Gallium Arsenide (GaAs) and Cadmium Sulphide (CdS). One way to obtain such materials is through the doping of Group IV elements with groups III and V, as shown in Fig. 1.2

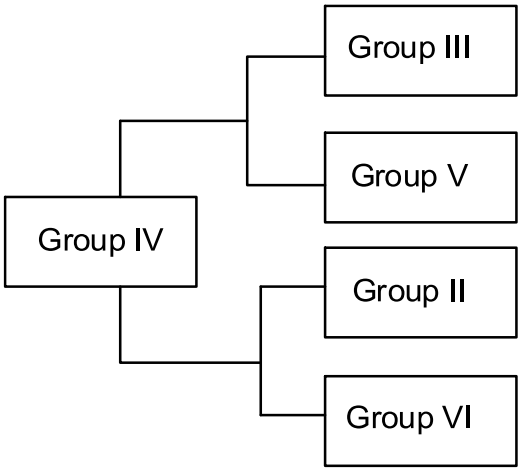

Figure 1.2: Chart of binary semiconductor formation (Liu et al., 2016; Mouhat and Coudert, 2014).

They can also be formed by inducing group II and VI elements in group IV of the elementary periodic table (RVelavan and Myvizhi, 2018). They crystallise into two main crystal structures, that is, zinc blende and wurtzite (Roknuzzaman *et al*., 2017). Despite their bonding structures being more ionic, zinc blende and wurtzite still maintain covalent bonding with high stability and strength (Mathematics, 2018). The diagram in fig 1.3 below shows the wurtzite binary crystal structure of Gallium Nitride (GaN) (Berends et al., 2019).

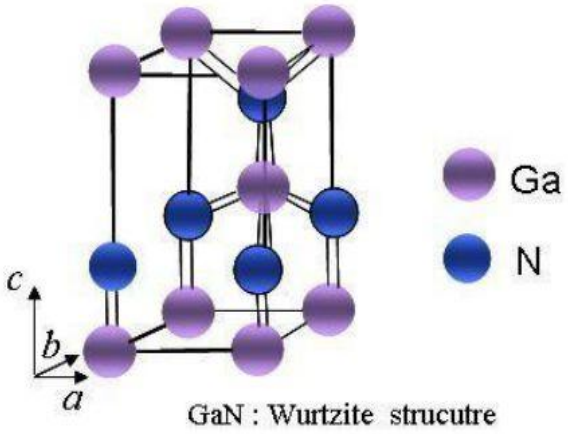

Figure 1.3: Gallium Nitride (GaN) Wurtzite binary semiconductor with dimensions a × b × c (Jaffe and Zunger 1984).

1.3.2 Ternary Semiconductors.

Ternary semiconductors comprise three elements in a periodic table. They are formed by either of the following ways, as shown in Fig.1.4 (Mathematics, 2018).

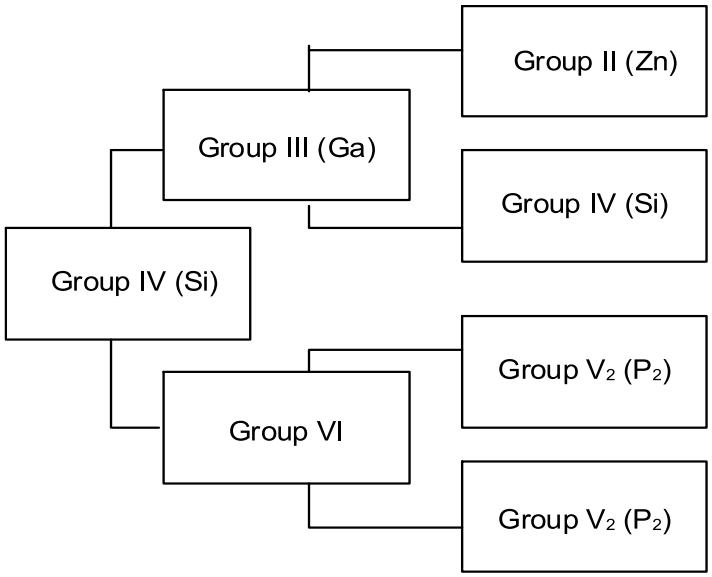

Figure 1.4: Ternary semiconductor formation using elements in different groups (Mathematics, 2018).

1.4 The Ternary Chalcogenides Semiconductors

There are two main types of ternary chalcogenide semiconductors, chalcopyrites and pnictides (Smith, 1975).

1.4.1 Chalcopyrites.

Ternary chalcopyrite semiconductors materials have a general formula $A^{I}B^{III}C_2$ where the superscript refers to the group of the element where it belongs. They are isoelectronic analogues of groups II-VI binary crystal structures (Irfan et al., 2021).The semi-conductivity properties of ternary chalcopyrite semiconductor materials can be determined by maintaining a total of four valence electrons in each atomic space of the structure. This is done by substituting groups I and III for group II, as per the Grimm-Somerfield rule. Most chalcopyrite compounds exhibit a wide energy spectrum. This is the main reason why these materials are suitable for application in photovoltaics, optoelectronics, microelectronics, magnetic fibre storage, spintronics, etc. Examples of Ternary chalcopyrite semiconductor materials include CuInSe2, CuGaS2 and AgInS2. The crystal structure of CuInSe2 as one of the examples of chalcopyrite is shown in the figure (1.5b) (Mathematics, 2018)

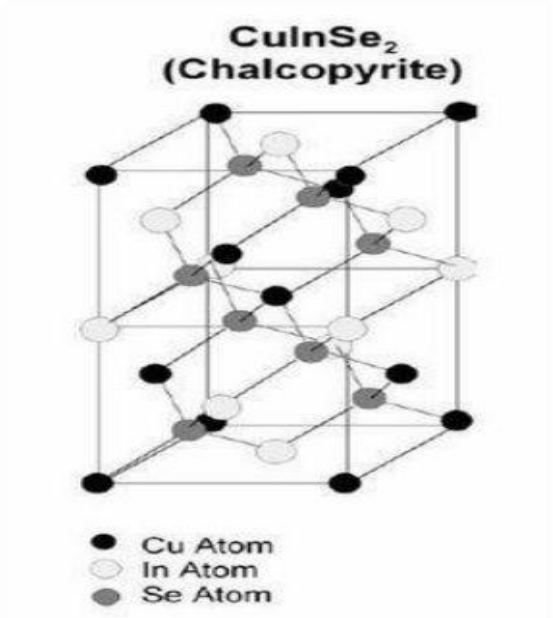

Figure 1.5: Crystal structure of CuInSe2 (Mathematics 2018).

1.4.2 Pnictides Ternary Semiconductors.

Pnictides Ternary semiconductor materials have the general formula $A^{II}B^{IV}C_2^V$ where A = K, B = Zn, Cu etc., and C = P, As and the superscripts refers to the groups of the named elements. Pnictides are analogues of group III-V isoelectronic binary semiconductor crystal structures. They form tetragonal

crystals with a space group of I-42d connected to the structure of zinc blende. The semi-conductivity of pnictide structures can be obtained by the substitution of groups II and IV for group III, and there must be four valence electrons on each atomic site of the structure according to the Grimm-Sommerfeld rule (Irfan et al., 2021).

Examples of pnictide ternary semiconductor materials are Zinc Sulphide diphosphate ($ZnSiP_2$) and tetra potassium di-arsenido zincate (K_4ZnAs_2), .The crystal structure of Zinc Sulphide diphosphate($ZnSiP_2$) is shown in figure (1.6) (Mathematics, 2018).

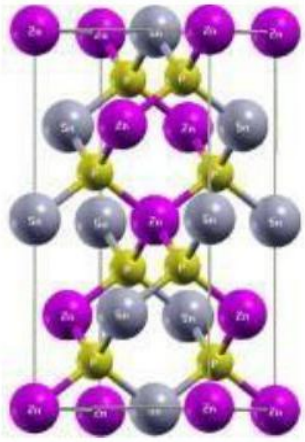

Figure 1.6: Crystal structures of Zinc Sulphide diphosphate ($ZnSiP_2$) ternary phosphate semiconductor materials (Mathematics 2018); (Prots et al. 2007)

Ternary chalcopyrites and ternary pnictide semiconductor materials have received excellent scientific research attention because of their unique crystal structures and exemplary physical properties such as high refractive indeces, nonlinear susceptibility, fairly excellent thermophysical and thermal electrical properties, wide physical spectrum, and high melting and boiling points (Zeb et al., 2020). These peculiar properties give ternary chalcopyrite and ternary pnictides opportunities for extensive research in the application of optoelectronics, sensor detectors, and optics solar energy/perovskites (Zeb et al., 2020).

1.4.3 Crystal Structure of Tetra-Potassium di-Arsenido Zincate (K4ZnAs2)

Tetra potassium di asenido-zincate forms a trigonal structure that belongs to a space group 166 and point group -3m.It was obtained in the form of a black crystal, plate-like structure, by reacting Tetra potassium diasenido-zincate (K_4ZnAs_2) and Tripotasium Arsenide (K_3As) at a temperature of 923 K for 4 h in a crucible and then placed in a steel ampule for cooling to a low room temperature (Prots et al., 2007).

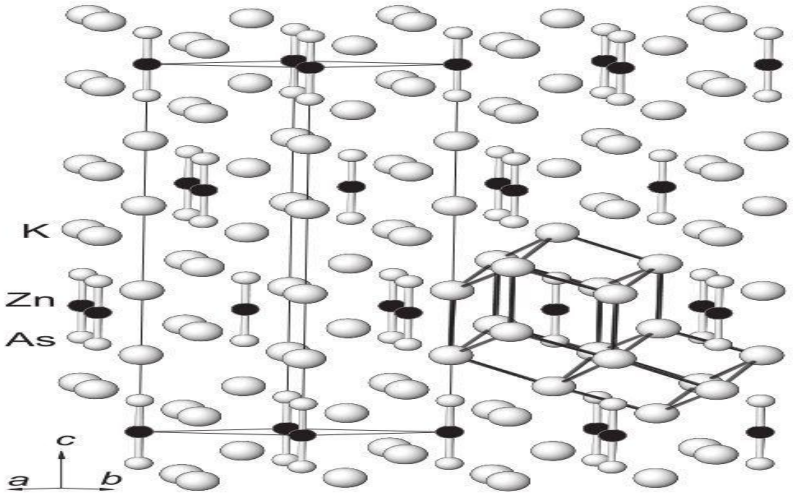

Figure 1.7: Crystal structure of tetra potassium diarsenido zincate (K_4ZnAs_2) (Prots et al. 2007)

1.5 *Ab Initio* Calculations

The research work can be done either experimentally in the laboratory, field work surveys, or through DFT simulations which involve the use of computer software codes. DFT material simulations help in the general prediction of material properties. This is always done by comparing the calculated results with the one done experimental results. The ab initio studies involve accurate approximations which are used to solve the Kohn-Sham discussed in chapter three. During the study of material properties, several codes aid in the calculations of many formalisms (Jeong et al., 2021).

From the standard elementary periodic table, different correlation functional properties of each element are accessed from the Material Cloud project by downloading the required elements, after which DFT parameters such as energy, density, band gap, and volume are created in various forms. It involves choosing a particular structure and creating all the data about the structure, for example, energy optimisation, lattice parameters, phonon dispersion graphs, and band structures (Giannozzi et al.,2009).

Fig 4.1, in Section 4.3, typically shows how the input file generated from the material cloud project looks like and the chart flow showing how the Kohn-Sham equations of a given structure are calculated in a (Giannozzi et al.,2009).

1.6 Statement of the Problem

Binary and ternary (chalcopyrites and pnictides) semiconductor materials have proved to have better properties that can make them be applied in photovoltaic and other photo electronic applications (Jeong et al., 2021) . The major disadvantage is the unclear information about the origin of their optoelectronic properties. Their potential in terms of efficiency, therefore, has not yet reached the level of the toxic Cd- and Pb-based semiconductor materials because of the stated limitation. The reason for this is there's little research work already done both experimentally and through the simulation method. Those that have already been done by simulations only few approximation functionals have been used to test convergences without considering the effect of overestimation and underestimation of the data. (Berends et al., 2019). In this work we investigated the insight on the structural, electronic, optical, mechanical and elastic properties of Zintl phased tetra potassium di arsenidozincate (K_4ZnAs_2) semiconductor compound by performing DFT simulations using ab initio studies to bridge the gap between the theoretical expectations and actual properties of this material using two exchange correlation functions functionals; the LDA and the GGA. The one based on LDA was Perdew-Zunger while those based on the GGA were Becke-Lee-Yang-Parr, Engel-Vosko, Perdew-Burke-Ernzerhof, Perdew-Burke-Ernzerhof for solids and Second-order correlations, (Berends et al., 2019). Doing this will help us propose for materials with better properties for solar energy harvesting.

1.7 Main Objective

To perform first-principles calculations on Zintl phased tetra potassium di-arsenidozincate (K_4ZnAs_2) semiconductor compound compounds for thermophysical and optoelectronic applications.

1.7.1 Specific Objectives

- To study the structural, optical, mechanical, and electronic properties of Zintl phased tetra potassium di-arsenidozincate (K_4ZnAs_2) pnictide ternary semiconductors.
- To study the mechanical and the elastic stability of Zintl phased tetra potassium di-arsenidozincate (K_4ZnAs_2) pnictide ternary semiconductors.
- To study the anisotropic properties of the Zintl phased tetra potassium di-arsenidozincate (K_4ZnAs_2) pnictide ternary semiconductors through the test of spatial dependence.

1.8 Justification and Significance of the Study

The potentials harvesting of pnictide ternary materials such as Zintl phased tetra potassium di-arsenidozincate (K_4ZnAs_2) semiconductors has not been fully realised for photovoltaic applications because of the little research work done on them leading to limited information regarding to the origin of their optoelectronic properties (Berends et al., 2 019). More and more research works are needed to bridge the gap between the theoretical expectations and actual material properties of ternary pnictides and identify efficient materials for the photovoltaic applications (Mbilo et al., 2022).

In this study, we performed first-principles calculations based on DFT, as structured in the quantum Espresso package, to investigate different properties of Zintl phased tetra potassium di arsenidozincate compound (K_4ZnAs_2). The PBE-GGA, PBEsol-GGA, LDA-PZ, BLYP-GGA, EVE-GGA, and SO-GGA functionals were used to achieve structural optimisation and applied for study of the structural, electronic, mechanical, elastic, and optical properties of the material (K_4ZnAs_2) compound. The results were compared with the one done experimentally to draw general conclusions. The research provided a clear information to the advanced options for more optimal performance of material-based devices which leads to commercialization and gradual movement to a cleaner and eco-friendly form of energy (Elenewskiand Hackett, 2012).

CHAPTER TWO: LITERATURE REVIEW

2.0: Introduction

The chapter contains a literature review of scientific work previously conducted by some scholars on both binary and ternary semiconductor materials based on ab initio molecular simulation tools. It has three sections; Section 2.1 has material modelling; 2,2 Solar Cell Efficiency 2.3 contain the review on the previous work while section 2.4 has a summary introduction of computational analysis which will be discussed in detail in chapter three while 2.5 has the detailed balanced limit.

2.1: Material Modelling.

Modelling is among the common methods used to study the general properties of most materials in both solid-state physics and applied chemistry (Körbel et al., 2016). This is often achieved by computational material design which provides insight and clear information about the structure of different materials for different applications. Parameters such as bond lengths, position and size of the band gap, lattice constant, orbital arrangements, trigonal distortions, gap level alignments, and anion displacement are very important when modelling a material for specific use (Burke, 2007).

The aim of material modelling is to optimise some properties, such as optical and other aspects, such as costs and material stability under different environments. Computational material design addresses these challenges because it is flexible to study and engineer the technological fabrication of materials of known complexity (Körbel et al., 2016). Computer-based atomic and molecular codes play a vital role by providing important energetic and structural characteristics of the atoms that make up the structure of the material. It combines factors such as quantum chemistry, solid-state physics, and statistical mechanics to highlight well-elaborated strengths and weaknesses to aid in the design of materials. Computer modelling of materials has been used to study various materials in scientific research with the main focus of obtaining an alternative energy source with the view of medicating global warming effects.

In most of these studies, the method provides simulation outcomes which often collaborate with the experimental data. Computers perform tasks, such as complex mathematical equations, which cannot be solved by seasoned mathematicians using artificial intelligence and machine teaching (Malakkal et al., 2016).It can manipulate theories that are very difficult to understand. This complements the experimental data and can be applied in the prediction of the properties of materials which are yet to be introduced in the field of material science.

Starting with an atomistic model, modern techniques can display the ground state structure, elaborate properties, and arrangement of electrons in the structure (Physics et al., 2020). A summary of the previous theoretical work is discussed in the subsequent sections.

2.2: Solar Cell Efficiency

This quality is very important to consider when choosing optoelectronic devices. It is the quantity the light energy that can be converted to useful electrical energy by a solar cell material when directly exposed to sunlight. Several factors determine the solar-cell efficiency of a material. An example is the cell geometry with respect to solar energy rays, temperature of solar energy, solar shading, etc. (Irfan et al. 2021). Figure 2.1 shows different efficiencies of different materials used in a solar cell; silicon based, organic photovoltaics, Dye sensitised solar cells (DSSC) and Photovoltaic solar cells (PSC) through the years.

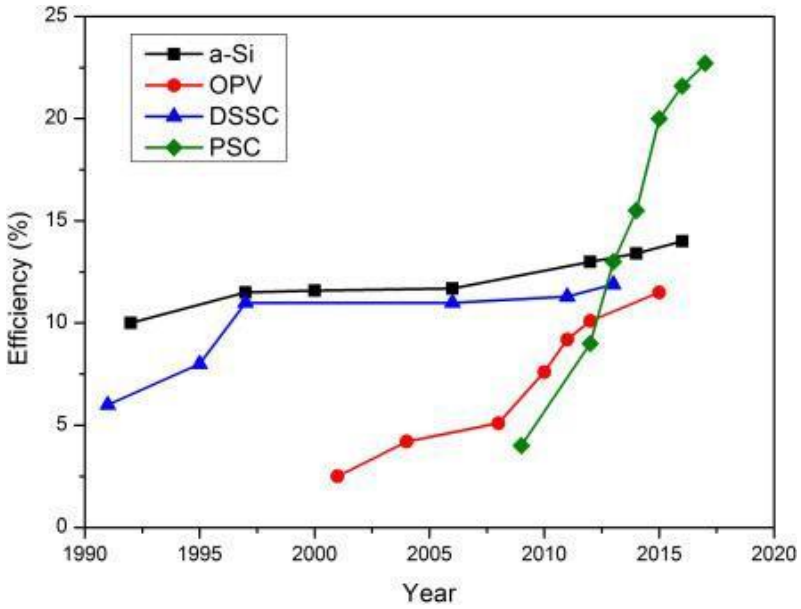

Figure 2.1 The graphs of efficiencies of different solar panels, (Sundaram *et al.*, 2018).

In the figure above, it is seen that the efficiency of Photovoltaic solar cells (PSCs) has drastically gone high over some years. This is because there have been several studies that have been carried out to source for the better materials required for photovoltaic thin film fabrications (Sundaram et al., 2018).

2.3: Review on the Previous Work

The elaborated study of groups I and II ($A^{I}B^{III}C_2^{VI}$ and $A^{II}B^{IV}C_2^{V}$) ternary semiconductor materials have been carried out as reported in various studies. Mbilo et al., 2022 performed Ab Initio study of tripotasium tricopper diphosphate ($K_3Cu_3P_2$) for solar cell applications.

Elenewski and Hackett, (2012) used a generalised gradient approximation with Hubbard parameter (GGA+U) approach supplemented with localized correlation to study the total electronic correlations of thiolate-ligated iron-oxo (IV) porphyrin. In comparison with the structure of the Hamiltonian model, they discovered that the moment of iron in 3d introduced correlation to the vicinity of the electrons making the local moments strong (Elenewski and Hackett, 2012).

Zeb et al., 2020 studied the structure of $K_3Cu_3P_2$ and K3Ni3P2 ternary pnictides semiconductor materials using first principles calculations and prospects density functional theory of for thermophysical and optoelectronic applications through optimization of structure of the materials incorporated in GGA with Perdew-Burke-Enzenhorf (PBE) as the correlation and exchange functional of energy (Zeb et al., 2020). Both $K_3Cu_3P_2$ and K_3Ni3P_2 materials displayed direct band gap semiconducting properties and their band gap values, both spin up and spin down, ranges from 1.7eV to 1.9eV (Zeb et al., 2020).

R.C Smith investigated on the general progress in application of groups I and II (AIBIIIC_2^{VI} and AIIBIVC_2^{V}) ternary semiconductor materials. The work studied both the optical and electrical responses of many compounds of II-IV-VI2 at room temperature. An example of such compounds is CuAlS2,CuGaSe2 etc (Smith, 1975).

Sree Parvathy et al., 2016 studied the thermoelectric properties of zinc based ternary pnictide semiconductors using first principles calculations and prospects of density function theory. They reported on the both electronic structure and the transport properties of several zinc based ternary pnictide semiconductors of the family ZnXPn2 (X=Si, Ge and On=P and As) and ZnXP2 (X=Si, Ge and An) (Sreeparvathy et al., 2016).Using DFT calculations and prospects, Jaffe and Zunger, (1984) studied the electronic structure of ternary pnictide semiconductors (ZnSiP2, ZnGeP2, ZnSiAs and MgSiP2). The trends in both band gap and bonding structure plus the charge distribution within the structure was studied (Jaffe and Zunger, 1984). Naher and Naqib, (2022) recently used first principles calculations and prospects of DFT to investigate the effect of individual atoms on both the binary and ternary semiconductor materials.

Through their investigation, the band structures was used in classifying the material into metal, insulator and semiconductor crystal structures (Naher and Naqib, 2022). Berends et al., 2019 investigated optoelectronic properties and prospects of ternary I-III-VI2 semiconductor materials. They provided an elaborated insight on the optoelectronic characteristics of compounds of group I-III-VI2. All materials displayed a large stroke shifts, broad bandwidth and long excitation life time (Berends et al., 2019).

Sergey et al., 2021 studied the Second harmonic generation (SHG) and birefringent properties of Ternary pnictide semiconductors of the general formula ABC2 (A=Zn,Cd, B=Si,Ge and C=As,P) using first principles calculation of the density function theory. They used computational method based on linear muffin tin orbital (LMTO) (Ou et al., 2021) .

Omata et al., 2015 investigated the wurtzite based ternary semiconductor materials of groups' I-III-O2 using first principles calculations and prospects of density functional theory. The magnetic properties, band gap structures, electronic configuration of elements in the structure of wurtzite materials, optical properties both in visible and UV regions were studied.

In this research work, basing on the first principles method, we investigated the structural, electronic, optical, mechanical and elastic properties on Zintl phased tetrapotassium diarsenidozincate K4ZnAs2semiconductor compound using the PBE-GGA, PBEsol-GGA, LDA-PZ, BLYP-GGA, EVE-GGA and SO-GGA functionals theory as implemented in quantum Espresso package (Perdew, et., al. 1965). We used Material Project database to download the CIF (Crystallographic Information file) files. The downloaded CIF files were used to generate the input files from the material cloud website.

To optimize both lattice constants and atomic positions within the tetra potassium diarsenido zincate (K_4ZnAs_2) structure, various cell relaxations were done which were then used in the calculation of structural, mechanical, electronic and optical properties (Mbilo et al., 2022).

2.4: Computational Analysis.

The common tool used in the computation of electronic crystal structures both in the field of solid-state physics and applied chemistry is *ab initio* molecular simulation tool based on DFT which act on Kohn-Sham equation 2.1 given below using several approximations discussed in section 3.3 in chapter three. The foundation of density functional theory was laid down using Hohenberg-Kohn (H-K) theorem in the calculations of charge density of semiconductors (Elenewski and Hackett, 2012).

Most of these theoretical studies tend to ignore the d orbitals of cations within the structure and the electronic charge density of electrons is not self-consistent (Han et al., 2016). The electronic density is expressed as shown by the equation (2.1) to get the minimum energy.

$$\frac{\delta f[n(r)]}{\delta n(r)} = 0 \qquad (2.1)$$

Where n® is electronic density and $f[n(r)]$ is function.

The LDA and GGA approximation potential apparatus are used to incorporate the atomic interaction and exchange correlations within the whole structure. In the determination and prediction of properties of compounds, local energy potential which depends solely on the electronic density n® of particles in each point in the region is used. It fails when the particles of the materials undergo a constant rapid changes in molecules (Irfan et al., 2021). GGA is used to determine the electronic structure using functional which depend on both electron density n® and its first derivative in XC potentials(Naher and Naqib, 2022).

Since the band gaps of insulators are under estimated, when LDA and GGA are used, it can lead to connection of the Kohn-Sham DFT with Hubbard parameters U either as LDA+U and GGA+U to be applicable in the correlation energy potentials such as tran-blaha modified Becke Johnson in the form of TB-MB functions. Hubbard parameters are incorporated in both GGA and LDA because of coulomb force as a result of particle attractions/ repulsion within the atomic structures (Callow et al., 2021).The electronic, elastic, structural, mechanical and optical properties of the tetra potassium diarsenido zincate (K_4ZnAs_2) in quantum Espresso package using GGA-BLYP.GGA-EVE, GGA-SO, GGA –PBE, GGA-PBEsol and LDA-PZ functional approximations was studied in this work.

2.5: Detailed Balance Limit

It is also called Shockley-Queisser limit. It is a theoretical limit in solar cells that highlights the highest efficiency a solar cell made from a single p-n junction can have theoretically (Shockley and Queisser, 1961).The highest theoretical efficiency η is the ratio of the generated solar energy to the input power as given by equation (2.2). (Physics et al., 2020).

$$\eta = \frac{P_{max}}{P_s} = \frac{E_g Q_s}{P_s} \qquad (2.2)$$

Where $P_{max}$the maximum power output, P_s is the incident power, E_g is the band gap energy of the crystal structure and Q_s gives the number of absorbed photons (Shockley and Queisser, 1961).

From (2.2), the number of absorbed photons is given by equation (2.3) which is obtained from integration of the Planck's law ((Irfan et al., 2021).

$$Q_s = \frac{2\pi(kT_s)^3}{h^3c^2}\int_{x_g}^{\infty}\frac{x^2dx}{e^x-1} \tag{2.3}$$

Where h, T_s, k, , and c are the, Planck's constant, the solar temperature, Boltzmann's constant and the speed of light respectively. Finally, P_s is given by equation (2.4)

$$\mathbf{P_s} = \frac{\mathbf{2\pi(kT_s)^4}}{\mathbf{h^3c^2}}\int_{\mathbf{0}}^{\infty}\frac{\mathbf{x^3dx}}{\mathbf{e^x-1}} \tag{2.4}$$

Applying the fact that

$$\int_0^{\infty}\frac{x^3dx}{e^x-1} = \frac{\pi^4}{15} \tag{2.5}$$

Equation (2.5) becomes equation (2.6), that is;

$$P_s = \frac{2\pi^5(kT_s)^4}{15h^3c^2} \tag{2.6}$$

Figure (2.4) displays the graphical representation of the detailed balance limit.

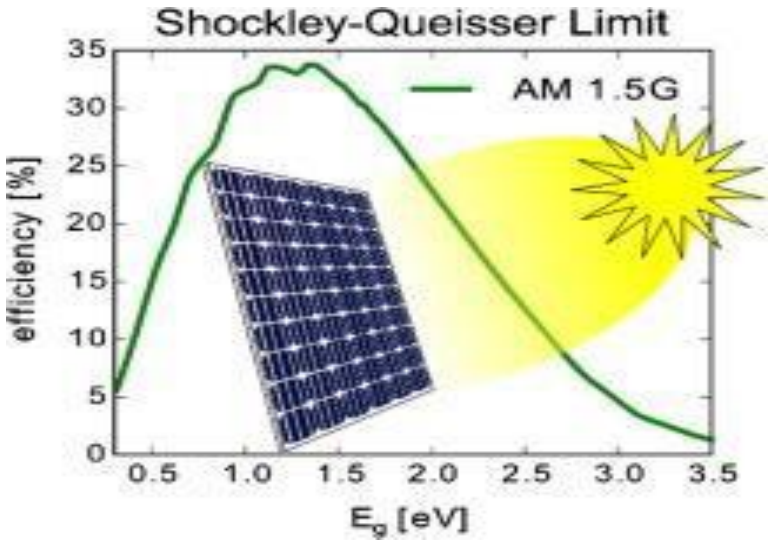

Figure 2.2 Graphical representation of the Shockley- Queisser limit (Rühle, 2016)

CHAPTER THREE: THEORETICAL FRAMEWORK

3.0 Introduction

Any material on Earth, whether in a solid, liquid, or gas state, is composed of many particles, such as atoms, ions, and molecules sandwiched together by strong electric forces. The arrangement of particles within the structure under the influence of these electric forces forms three states of matter (Talirz et al., 2020). The behaviour of these many particles in a body can be well explained using the many body Schrödinger wave equation (Bretonnet, 2017). The Schrödinger equation has a Hamiltonian which constitutes the kinetic energy, effective potentials, and interaction of the particles. Despite the simplicity of Schrödinger's equation, it is very difficult to obtain solutions (Giannozzi et al., 2009). Density function theory is used to look for possible solutions to the Schrodinger equation using a set of physical approximations called *ab initio* molecular simulation tools, also called first-principle calculation approximations (Physics et al., 2020). This chapter contains the theoretical framework of some approaches used to determine possible solutions to the Schrödinger wave equation. It has four subsections, including the background of DFT, computational theory, first-principles calculations, and approximation for the exchange correlations of energy.

3.1 Background of Density Function Theory

Atomic particles consisting of a positive central nuclear core and negatively charged electrons (both ground-state and valence electrons) play a very important role in determining the general characteristics of the crystal structure. However, understanding the general behaviour of these particles within the structure is extremely difficult because most of their parameters are very complex, as described by the Schrödinger wave equation (Sholl and Steckel, 2009).. Much research is underway on various theories with the aim of gathering enough information to obtain lasting solutions of the Schrödinger equation which describes the basic behaviour of these atomic particles in external Coulomb fields. The non-relativistic time-independent Schrödinger equation is denoted by equation (3.1) (Schrödinger, 1926; Zerfass, 2015).

$$\mathbf{H\Psi = E\Psi} \qquad (3.1)$$

where H is Hamiltonian denoting the total energy of the system and Ψ denoting the wave functions of the many body system (Burke, 2007).

For a system of several electronic particles (electrons and nuclei), the Schrodinger equation is given by equation (3.2) (Burke, 2007).

$$\hat{H}(r_1, r_2 \ldots r_N ; R_1, R_2 \ldots R_M) = E\Psi(r_1, r_2 \ldots r_N ; R_1, R_2 \ldots R_M) \quad (3.2)$$

where r and R_s denotes the coordinates of electrons and nuclei in the atomic structure respectively and ψ is the wave functions of the particles in the structure.

The Hamiltonian operators have the total kinetic energy and effective potential energy given by equation (3.3) (Burke, 2007)..

$$\psi(T + V) = E\psi \quad (3.3)$$

where T is the total kinetic energy and V is the effective potential energy of the electron-electron, electron-nuclei and the nuclei-nuclei interaction within the atomic structure. Putting equation (3.2) to (3.3) we've

$$\hat{H} = T_e + T_n + V_{e-e} + V_{e-n} + V_{n-n} \quad (3.4)$$

Tackling and getting the solution of equation (3.4) of many body systems of particle is very difficult because we are handling the spatial coordinates which requires us to consider each particle in 3D. This becomes more complex when handling the interparticle interactions ((Schrödinger, 1926; Zerfass, 2015).Various first principles approximations is put forward to find the solution of many bodies system of S.E problem (Zerfass, 2015).

3.2 First Principles Calculation Approximations

The first principle, based on the interaction of particles within the atomic structure according to quantum mechanics principles, tries to look for a solution of the Schrodinger equation through a series of approximations to obtain eigenvalues and eigenfunctions of the body system and thus its electronic structure. Below are some of the approximations that have been proposed by different scholars trying to simplify the Schrödinger equations of a many-body system (Sholl and Steckel, 2009) .

3.2.1 The Born-Oppenheimer Approximation

In a body, the interacting system of valence electrons and cantered nuclei transfers minimal momentum to each other because the two have different masses and experience different Coulomb forces of attraction.

However, the Coulomb forces of attraction between them remain constant, because they have opposite charges. Based on this, if one imagines that the momenta of these oppositely charged interacting system particles are equal, then the nucleus should have almost zero velocities because they are very massive compared to electrons.

The assumptions under the Born–Oppenheimer approximation is the motion of both nuclei and electrons within the molecule that are separated, leading to separated molecular wave functions in terms of electron and nuclear positions. On the scale of nuclear motion, the valence electrons are said to relax in the ground state, as given by the Hamiltonian equation (Sholl and Steckel, 2009) . This approximation which separates the nuclei and electrons within the structure by neglecting the contribution of nuclear energy to the kinetic energy in the general Schrödinger equation, is called the Born-Oppenheimer approximation/adiabatic principle.

The total energy involves the kinetic energy of the interreacting electrons and the Coulombic forces of repulsion between electron- electron interactions, electron -ion interactions, ion- ion interactions, and electrons of many bodies, but not nuclei-based interactions (Physics et al., 2020). The general Schrödinger equation is now reformulated by this approximation as equation (3.5) (Burke, 2007).

$$\hat{H} = \hat{H}_N + \hat{H}_e \qquad (3.5)$$

The Hamilton of both the potential and kinetic energy as a result of the interaction of the system of electrons is given by equation (3.6).

$$\hat{H} = T_e + V_{e-e} + V_{e-n} \qquad (3.6)$$

The Born-Oppenheimer approximation is applied in the simplification of the time-independent Schrodinger equation of many-body systems by concentrating on the electronic particles only (Toulouse, 2019). Dealing with the interactions of electrons only within the structure, the time independent Schrodinger equation becomes (3.7) (Sholl and Steckel, 2009).

$$\hat{H}(r_1, r_2 \dots r_N) = E\Psi(r_1, r_2 \dots r_N) \qquad (3.7)$$

Where I is the wavefunction Ψ and is given by equation (3.8).

$$\Psi = (r_1, r_2 \dots r_N) \qquad (3.8)$$

From the time-independent Schrodinger equation in equation (3.8), the electronic Hamiltonian gives (3.9) (Sholl and Steckel, 2009).

$$(T_e + V_{e-e} + V_{e-n})(r_1, r_2 \ldots r_N) = E(r_1, r_2 \ldots r_N) \tag{3.9}$$

And from this can be expanded to have equation (3.10).

$$\left[\frac{h^2}{2m}\sum_{i=1}^{N}\nabla_1^2 + \sum_{i=1}^{N}V(r_i) + \sum_{i=1}^{N}\sum_{j<1}U(r_i, r_j)\right]\Psi = E\Psi \tag{3.10}$$

From Equation (3.10), the electron- electron interaction is still complex in solving the equation. This is where the DFT steps to obtain the solution.

3.2.2 Hartree Fork Approximation

This is also called independent particle approximation. The resulting equation after the Born–Oppeheimer approximation acting on the Schrodinger equation is in fact more complex than before because the electron-electron interactions inside the orbitals within the structure are ignored (Zerfass, 2015). (Allan, 2021). The Hartree fork approximation determines the wave functions and energy of the quantum properties of many-body particle systems in stationary states. It is postulated that the motion of each electron in the atomic structure is described by a single-particle motion called an orbital which does not depend on the motion of other particles (Burke, 2007). Hartree fork approximation works on the basis of simple approximation of many body wave functions given by a single state operator of N spin orbitals given by equation (3.11).

$$\Psi = \begin{vmatrix} \psi 1(X1)\psi 1(X2) \ldots \ldots \ldots \psi 1(XN) \\ \Psi 2(X1)\psi 2(X2) \ldots \ldots \ldots \psi 2(XN) \\ \vdots \\ \Psi N(X1)\psi N(X2) \ldots \ldots \ldots \psi N(XN) \end{vmatrix} \tag{3.11}$$

where x is the coordinates of spin and space, and Ψ is the wave function that provides the solution of the Hamiltonian.

The wave function under this approximation is symmetrical with respect to the change in all positions of electrons within the structure, and they obey Pauli's exclusion principle given by equation (3.11) (Zunger and Wei, 1996).

$$\Psi(X_1, X_2 \ldots . X_i, \ldots \ldots X_j \ldots . X_N) = \Psi(X_1, X_2 \ldots . X_i, \ldots . . X_j \ldots . . X_N) \quad (3.12)$$

3.2.3 Density Functional Theory.

Under density function theory, one does not solve a very complex Schrödinger wave equation; instead, one solves a very simple and straightforward formulation based on the Pierre Hohenberg and Walter Kohn theorem which states that the total energy and other parameters within the atomic structure are determined by the ground state probability of the election density (Bretonnet, 2017).

DFT approximations eliminate the complexities posed by the Hartree-fork formulation by considering both the energy exchange and correlation within the atomic structure. It determines the ground-state electronic structure of the wide properties of all kinds of atomic particles. It lowers the Schrödinger wave equation by solving the Kohn-Sham equation and its function (Toffoli, 2012). The ground-state energy of identical fermion particles is a special function of particle density, and its electronic state resembles a fully solved Schrödinger equation. This minimises the energy of the overall function. This functional attains its threshold value with respect to the change in particle density subjected to the normalised condition as long as the density has its correct values (Bretonnet, 2017).DFT is a type of first-principles calculation, named so because it can predict the properties of various particles, both known and unknown or real and ideal, without necessarily requiring experimental input (Toffoli, 2012).

This requires low effort while performing computational exercises. Computational exercise focuses on the whole electron density system to perform atomic modelling for any structure in a periodic table, both in elemental and molecular or compound states. Using a supercomputer, one can perform the modelling of several particles without necessarily going to the laboratory to perform experiments. A DFT user can easily relate the experimental measurements to the simulated results and draw lasting conclusions about the general properties of various compounds (Physics et al., 2020). In 1976, Hohenberg and Kohn discovered that the sum of the number of particles and their total energy can be calculated for a group of atoms in an external potential field as long as the external potential is a known function of the density of states, which is also proposed by DFT (Zunger and Wei, 1996).

3.2.4 The Hohenberg- Kohn (H-K) Theorems

The Hohenberg and Kohn theorems came into DFT by indicating that the function of the density of states contains all the properties required by the system of particles in a compound, and it is less complicated because the density of states has only three coordinates (Burke, 2007). Therefore, it is very easy to solve system of many-body problems. In DFT, the Hamiltonian operator interacts with electronic particles and has an external potential which mostly involves the nucleus-electron interactions. Since there is mapping of the potential and the ground state density of particles (Burke, 2007) , that is equation (3.13).

$$v(r) \longrightarrow n(r) \qquad (313)$$

Hohenberg and Kohn indicated that the inverse is true; that there is a mapping from the ground state density to the potential given by equation (3.14) (Zunger and Wei, 1996) .

$$n(r) \longrightarrow v(r) + Const \qquad (3.14)$$

Thus, it is clearly seen that the ground state density determines the potential (Harrison, 2005). . The Hamiltonian of the system of particles provides complete information on the system of particles.

The Hohenberg- Kohn theorem was first proven using the contradiction method. It was shown that the ground-state energy of possible electronic particles in a material is a unique functional. Hence, Density Function Theory (DFT) is used. The main drawback of this theorem is that, after postulating the existence of an energy functional, it does not specify the exact definition of the functional proved (Sholl and Steckel, 2009). The other Hohenberg-Kohn theorem is the second theorem which probes if a given density of states is in the ground state density ρ_0. This optimisation is performed based on the variational principle, where the trial density of states is used to determine the lowest possible minimum energies.

3.2.5 Kohn-Sham Equation

Schrödinger equation in the ground state of ideal non-interacting particles gives the same density of state as that of interacting particles (Burke, 2007). Burke (2007) reformulated the Schrödinger equation of a much-body system such that it has a Hamiltonian similar to that of interacting particles. Reformulating the Schrödinger equation from the H-K theorems, the energy exchange functionals can be expressed by equation (3.15) (Harrison, 2005):

$$E[\rho] = T[\rho] + V_{ext}[\rho] + V_{e-e}[\rho] \qquad (3.15)$$

The energy in the ground state and other observables can be easily computed given their exchange correlation (Widyastuti et al.,2022). The effective potential in atomic units is given by equation (3.16).

$$V_{eff} = V_{ext}(r) + V_H[n(r)] + V_{XC}[n(r)] \quad (3.16)$$

Where Veff is the effective potential, Vext[n(r)] is the external potential, VH [n(r)] is the Hartree term, VXC [n(r)] is the exchange correlation term, and n(r) is the electron density (Burke,2007). This leads to a new reformulated Schrödinger equation for the Kohn-Sham Equation (3.17) (Bretonnet, 2017).

$$H\psi = \left[\frac{-1}{2}\nabla_i^2 + V_{eff}\right]\psi_i(r) = \varepsilon_i\psi_i(r) \quad (3.17)$$

Where H is Hamiltonian operator, Veff(r) is effective potential, εi is minimum energy and Ψi is many body wave functions. From the energy functional, the K-S equations are expressed as (Sholl and Steckel, 2009.);

$$\left[\frac{h^2}{2m}\nabla^2 + V(r) + V_H(r) + V_{XC}(r)\right]\Psi_i(r) = E_i\Psi_i(r) \quad (3.18)$$

From the K-S equation above, notice that it differs from the S.E because we are dealing with individual electrons. VH is the Hartree potential and VXC represents the exchange and correlation potential.

3.2.6 The Self Consistent Field (Scf) Cycle

The Hamiltonian operator of the Schrödinger wave equation has both the kinetic energy and effective potential energy of the particles Veff. Veff of the particles in the structure depends on the electronic density and can be calculated from wave function Ψ. The flow chart in figure (3.1) displays how the K-S equation can be solved for frozen nuclear particles. This is done by optimizing the cut-off energy and k-points of the sample which determines the nature of the pseudo potential to be used. By taking the trial electron density n (r), which is directly proportional to the energy ground state E0, as an input to the effective potential, a new effective potential is obtained, which is consistent with the previous trial density. This process makes the density of states self-consistent (Sholl and Steckel, 2009).

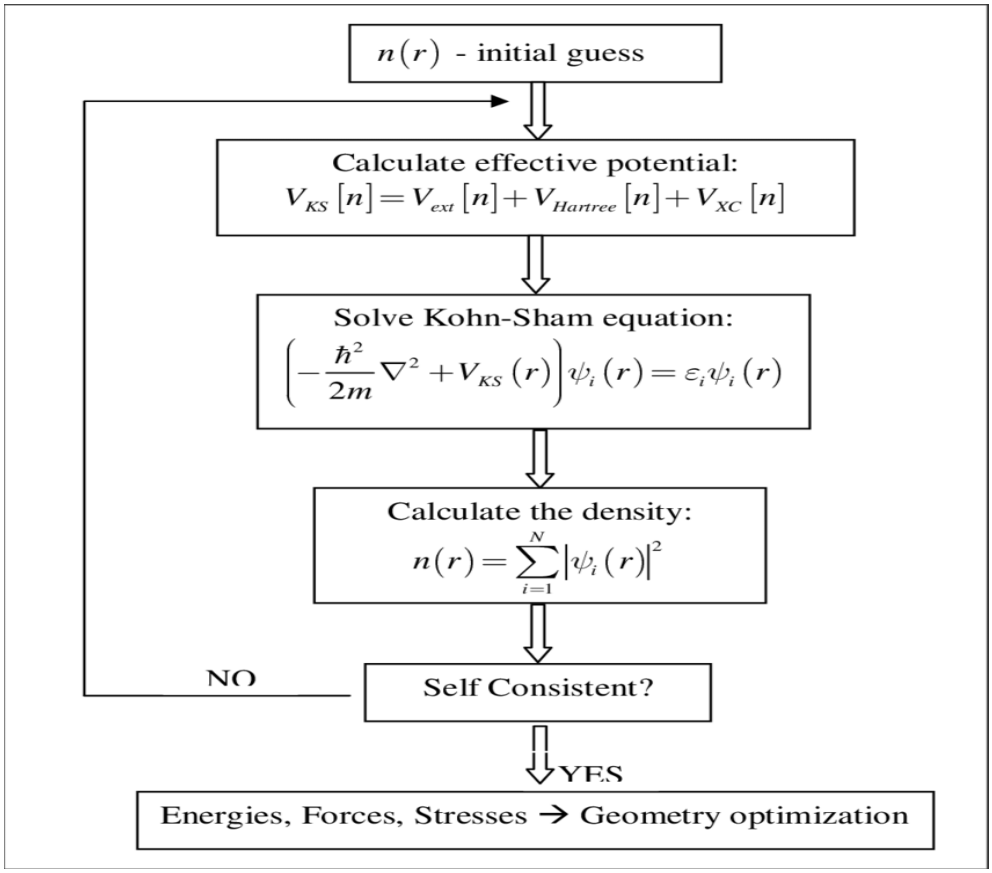

Figure 3.1 The Kohn-Sham equation self-consistence flowchart (Burke et al., 1997).

3.2.7 DFT with Coulomb Interaction (Dft+U)

The Hubbard model which was primarily used as an ad hoc method designed to describe the XC energy of the extended ground state of the d and f electron orbitals of transition elements, falls under the DFT intra-atomic interaction of particles within the atomic structure.

This model adds a Hubbard-like component to the Coulomb force of the interacting particles within the structure. Its overall energy is the sum of the GGA energy given by equation (3.19) (Giannozzi et al., 2009).

$$E_{DFT+U}[n] = E_{DFT+U}[n] + E_U \qquad (3.19)$$

3.3 Approximation for Exchange Correlation Energy

Computing a solution for the Schrödinger equation in ground-state particles in a much-body system is very difficult. This is because, when solving the familiar Kohn-Sham equation, the exchange-correlation functional of the interacting particles must be known which is not always clear. The homogenous electron gas provides a clear approach for solving the Kohn-Sham equation. Examples of these approaches include the local density approximation (LDA), generalised gradient approximation (GGA), local density approximation + Coulomb interaction (LDA+U), generalised gradient approximation + Coulomb interaction (GGA+U), and pseudo-potential approximations (Dorado et al., 2009).

3.3.1 Local Density Approximation

LDA is an example of the XC functional in the ab initio calculation of DFT which describes the properties of many body systems, such as phase stability, vibrational frequencies, structure, and elastic modulus. It depends entirely on the density of electrons and not on the electronic derivatives or K-S orbitals. Successful LDAs include those with derivatives of the HEG model. They are more important in the generation of more complicated approximations of XC energy. Using LDA to calculate the energy difference of a two-body system has many errors, such as the overrated binding energy. The exchange co-relation energy of each electron in electronic gas homogeneity has a density similar to of that the electron gas at any point **r** given by equation (3.20) (Dorado et al., 2009).

$$E_{XC}^{LDA}[n(r)] = \int \epsilon_{XC}[(n)]n(r)d(r) \qquad (3.20)$$

3.3.2 Generalized Gradient Approximation

To improve the DFT calculations, GGA was used to take the position of the fluctuations in the density of states. The formulation was proposed by Perdew and Wang. It depends on the electronic density and derivative/gradient at a given point. GGA reduces the error of energy atomisation of all sets of molecules comprising suitable light atoms by an appropriate factor, 4 which equates to an error of approximately 2-3 kcal/mol. GGA yields relatively accurate results even with binding energies. It fails when the electronic density-like molecules undergo constant rapid changes (Burke et al., 1997).

$$E_{XC}^{GGA}[n(r)] = \int d^3rf \qquad (3.21)$$

3.3.3 The Perdew, Burke, Ernzerhof (Pbe) Exchange-Correlation Functional

The PBE-GGA exchange correlation was proposed by Perdew, Burke, and Ernzerhof. It is a simple approximation of the GGA for the exchange and correlation energies of electronic particles. It works well, especially when molecules interact with the metal surfaces. It is very reliable for bulk calculations of the n(r) and XC energies. When used in bond energy calculations, PBE is among the most applied functions because it reduces the mean absolute error to reasonably meaningful accuracy. It will be used in this research because it conserves several features, both in exchange parts and correlation. However, when applied to the determination of the bond length, it overrates it. Therefore, has several errors thanLDA (Giannozzi et al., 2009).

3.3.4 Pseudo-Potential Approximation

They are also called the ideal effective potential and are used as an approximation to simplify complex systems. Pseudo potentials (Vps) are always used in place of electrons bounded on the core of an atom for effective improvement of calculations. Generally, it is assumed that the only particles which take part in chemical reactions and bonding processes are electrons, which are actively used in the analysis of the chemical and physical properties of atoms/elements. In this formulation, bounded electrons are assumed to be static, and the forces of attraction between ions are purely electrostatic in nature.This eliminates the need for inclusion of ground states and nuclear potentials which also participate in holding cloud electrons in the atomic structure (Sholl and Steckel, 2009.).

These strong core potentials are replaced with weak pseudo-potentials viewed as pseudo-wave functions instead of normal electron wave functions (Giannozzi et al., 2009).Therefore, it takes the place of the valence electrons. There are two sets of pseudo potentials: normalized conserving pseudo potential which normalizes the motion of electrons to be periodic, and the ultra-pseudo potential which lowers the sum of plane waves, making convergence of the density of states faster (Giannozzi et al., 2009).

The diagram shown in Figure 3.2 illustrates the full all-electronic (AE) wave function and the electronic potential. The valence electron wavefunctions move faster in the space having the inner-core electrons owing to the strong ionic potential. These movements have orthogonality between the inner core pseudo-wave function in the both inner core space electrons and the outermost valence electrons. The pseudopotential is designed such that no radial nodes exist in pseudo-wave functions and pseudo-potentials are always symmetrical to all electron wave functions, and the potential in the outer space of a radius cut-off care should be taken because the pseudo-potential may introduce the ghost state/nonphysical state within the system (Seitsonen, 2009).

3. 4 Computational Theory

Interacting particles in an atom are described in terms of qualitative models (quantum mechanics) improved from the semi-empirical classical mechanics. This is done using ab initio molecular simulation tools, also called first-principles calculations (Callow et al., 2021). The Schrodinger equation which forms the basis of interacting particles within the atomic structure, has a Hamiltonian that is composed of kinetic energy that comes as a result of electron-electron interactions and the potential energy as a result of electron-nuclear interactions. The first principle calculations reformulate Schrodinger equation to Kohn-Sham equation bearing the clear insight information of correlation effects of interacting particles (Fan et al., 2022). Naturally, an atom is composed of positive core nuclei surrounded by clouds of valence electrons. Nuclei and inner filled orbitals are often positively charged while the valence electrons are massless, faster moving and negatively charged.

Electrons near the nucleus are said to be bound to the ground state. The properties of electrons in the ground state of an atom are defined as those of definite, discrete N interact ing particles in an external potential Coulomb field generated by a series of nucleic configurations within the system (Giannozzi et al., 2009). These are considered to be fixed-point charges. Valence electrons are not specific to any particular core; instead, they move freely within the atomic structure and experience equal forces of attraction from each nucleus in the structure. These valence electrons participate in the bonding and chemical reactions (Bartolotti and Flurchick, 2007).Advanced research practices in solid-state physics are practiced from the classical point of view to the quantum point of view of particle interactions within an atom using first-principles calculations, also called first principle calculations.

Because the Schrödinger equation forms the foundation of the classical point of view of solids, the Hamiltonian of interacting particles has both the kinetic energy and effective potential V of the particles within the structure. The computational method involves changing the Schrödinger formulation to the Kohn-Sham formulation. From a microscopic point of view, a solid is seen to have positively charged cores (nuclei) cantered in a cloud of valence electrons and filled orbitals that are very massive and move slowly relative to electrons and are viewed as classical particles, while the valence electrons are viewed as massless particles moving very fast and are seen as quantum particles(Callow et al., 2021) .

CHAPTER FOUR: MATERIAL AND METHODS

4.0 Introduction

This chapter contains details on how the computational methods were performed on the trigonal crystal structure of Zintl phased tetra potassium di arsenidozincate K_4ZnAs_2 semiconductor compound. It has got five sections; section 4.1 has computational methods,4.2 highlights more about the pseudopotentials used in DFT calculations. Section 4.3 explains how the quantum espresso input file are applied in the DFT calculations. Section 4.4 has the explanation and equations used in the calculations of the optical properties while section 4.5 has the structural properties. (Giannozzi et al., 2009); (Mathematics, 2018) (Prots et al., 2007) are the main references used in this chapter.

4.1. Computational Methods

The computations in this work were carried out using the plane-wave self-consistence field method, PWscf, using the ab initio calculation method coded in the quantum espresso computational program which uses first-principles technique study (Giannozzi et al.,2009). The generalised gradient approximation method and the local density approximation method were used as the exchange-correlation potential (Ziesche et al., 1998), with two types of exchange-correlation functionals adopted for the work: ultra-soft-core correction with scalar relativistic type or the norm-conserving scalar relativistic type. The functional used for the local density approximation computation was the Perdew-Zunger LDA-PZ (Perdew and Zunger, 1981) while those based on the generalised gradient approximation used were GGA-BLYP (Becke-Lee-Yang-Parr) Miehlich et al.,1989, GGA-EV (Engel-Vosko) (Ziesche et al.,1998). GGA-PBE (Perdew-Burke-Ernzerhof) Perdew and Zunger,1981, GGA-PBESol (Perdew-Burke-Ernzerhof for solids) Perdew and Zunger, 1981, and SO-GGA (second-order GGA) (Zhao and Truler,2008). The procedure for obtaining the crystallographic information file and processing the input files has been described previously (Mbilo et al., 2022). The lattice parameters, kinetic energy cut-off and Monkhorst-Pack k-pont mesh were optimized, including the variable cell relaxation, before the actual cell computation were performed (Monkhorst and Pack, 2022). The optimized cut-off kinetic energy in relation to the total energy was set at 140 Ry, whereas the final Monkhorst-Pack k-point mesh used in this work was optimized at 9×9×9 with an offset of 0. Additionally, geometry optimization was performed by minimizing the total energy with respect to the lattice parameter and then fitting the data to the Birch-Murnaghan equation of state, as reported elsewhere (Mbilo et al., 2022).The optimum parameters were applied in the calculations of the band structures, density of states,mechanical, and optical properties of the compound material.

4.2 Pseudo potentials

The electrons in a solid crystal structure are categorized into two groups: inner core electrons and outer valence electrons (Giannozzi et al.,2009). The electrons in the core do not participate in chemical reactions and are in an inert state. Valence electrons participate in the chemical bonding and are mobile within the crystal structure. This implies that the valence electrons determine both the physical and chemical behaviors of the structure (Mathematics, 2018).

Therefore, much focus is put on valence electrons when studying the structure of a material. As the core electrons are fixed and inert, their effective potentials Veff are determined by replacing them with weak pseudopotentials which assume their effects. The pseudopotentials were downloaded from the Q.E website. The right pseudopotentials are chosen from the website, depending on the functionals used (PBE-GGA, PBEsol-GGA, BLYP-GGA, EV-GGA,SO-GGA, and LDA-PZ) (Prots et al., 2007). Pseudopotentials can also be generated from the Gbrv pseudopotential website (Prots et al., 2007) .Figure 4.1 below illustrates the pseudopotentials with the red dashed line showing the pseudopotential and the blue dashed line showing the psuodo wavefunctions of the system of particles (Råsander, 2010).

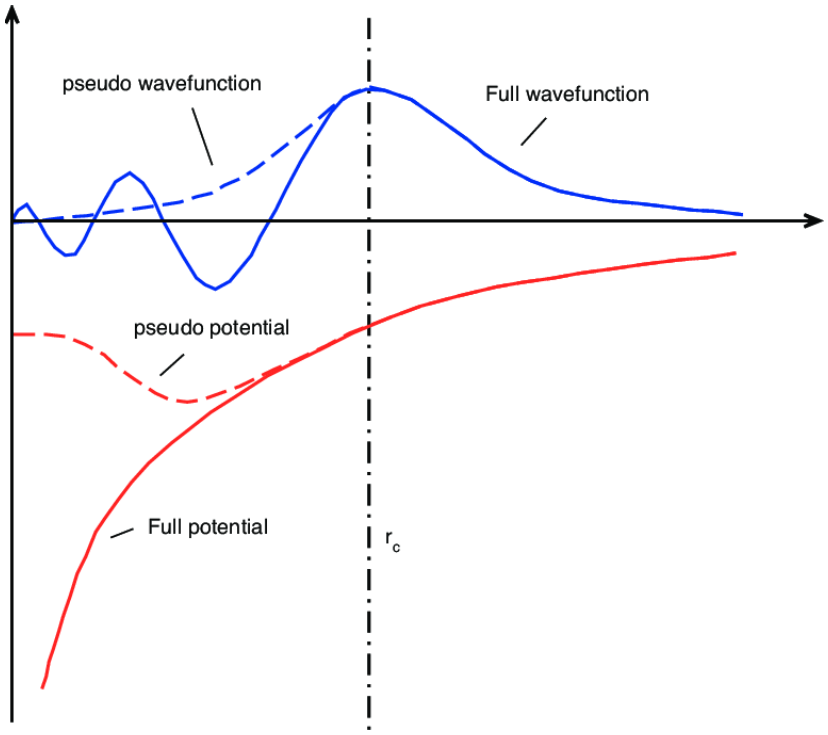

Figure 4. 1 Illustration of the Pseudopotentials, (Råsander, 2010).

4.3 The Quantum Espresso Input File

The quantum Espresso input files depend on the calculations that are performed. It can be used for scf, vc–relax, band structure computations, etc. Each file has special parameters required for first-principles calculations. From the standard periodic Table of Elements, the properties of each element are accessed from the Material Cloud project by downloading the required elements, after which DFT parameters such as energy, density, band gap, and volume are created in various forms. It involves choosing a particular structure and creating all the data about the structure, for example, energy optimisation, lattice parameters, phonon dispersion graphs, and band structures (Giannozzi et al.,2009). Fig 4.1 below typically shows how the input file generated from the material cloud project looks and the chart flow showing how the Kohn-Sham equations of a given structure are calculated in a quantum espresso (Q.E) package (Giannozzi et al.,2009).

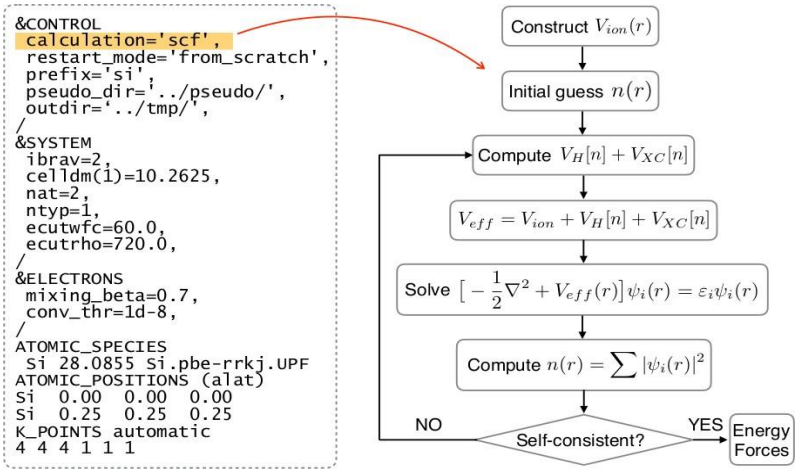

***Figure 4.2*. Kohn–Sham equation flow chart (Ciucivara, 2007).**

The %control, %system and the %electrons are the main name lists used in QE calculations. Atomic species and k-points are the main cards used in this package. The %control name lists used to indicate the flux of computation, the % electron name list has a specific system, and the atomic species indicates the type of atoms and the pseudopotential files used. The atomic position card indicates the position of the atoms in the structure (Giannozzi et al.,2009).

4.4: Optical Properties

The study of the optoelectronic properties of a structure is crucial because it explains the behavioural response of a crystal structure when it interacts with light energy (Saikia et al., 2022). The dielectric function comprises of the real and the imaginary components.

A complex dielectric function is used to study the optical properties of the material. It is represented by Equation (4.1) below (Giannozzi et al., 2009); (Mathematics, 2018), (Roknuzzaman et al., 2017).

$$\mathcal{E} = \varepsilon_1(\omega) + i\varepsilon_2(\omega) \tag{4.1}$$

where $\varepsilon_1(\omega)$ represents the real part and $\varepsilon_2(\omega)$ the imaginary part $\varepsilon_2(\omega)$ that can be generated from the Kramers- Kronig equation after finding the imaginary part of the function (Roknuzzaman et al., 2017). This function is dependent on the arrangement of the electronic band structures of a given material and affects its properties entirely (Kittel, 2005). Through the application of this dielectric function, the behaviour of the electronic bands within the structure can be studied (Mathematics, 2018).

The dielectric function can also be applied to investigate other optoelectronic properties of the material like the optical absorption coefficient, the extinction coefficient, Refractive index and the reflectivity.The optical absorption coefficient $\alpha(\omega)$ measures how photon energy passes through the material at different frequencies. It is generated from the dielectric function using the real and imaginary part of function as shown in equation (4.2) below (Kittel, 2005).

$$\alpha(\omega) = \sqrt{2}\omega\left(\sqrt{\varepsilon_1^2(\omega) + \varepsilon_2^2(\omega)} - \varepsilon_1(\omega)\right)^{\frac{1}{2}} \tag{4.2}$$

The extinction index $K(\omega)$ is related to the dielectric functions by in equation (4.3) (Saikia et al., 2022).

$$K(\omega) = \left(\frac{\sqrt{\varepsilon_1^2(\omega) + \varepsilon_2^2(\omega)} - \varepsilon_1(\omega)}{2}\right)^{\frac{1}{2}} \tag{4.3}$$

where $K(\omega)$ **is the** the extinction index.

The refractive index $n(\omega)$, which measures the bending of light energy as it traverses different media represented by equation (4.4) below (Kittel, 2005) .

$$n(\omega) = \left(\frac{\sqrt{\varepsilon_1^2(\omega) + \varepsilon_2^2(\omega)} + \varepsilon_1(\omega)}{2}\right)^{\frac{1}{2}} \tag{4.4}$$

The reflectivity $R(\omega)$ is connected to the refractive index by equation (4.5).

$$R(\omega) = \frac{(n-1)^2 + K^2}{(n+1)^2 + K^2} \qquad (4.5)$$

The energy loss $L(\omega)$ measures the amount of light energy loss as the photon energy undergoes absorption, scattering, radiation and reflection when it interacts with a material. It is given by equation (4.6) below (Saikia et al., 2022).

$$L(\omega) = \frac{\varepsilon_2(\omega)}{\varepsilon_1^2(\omega) + \varepsilon_2^2(\omega)} \qquad (4.6)$$

The refractive index and extinction coefficient in relation to the dielectric function $\mathcal{E}(\omega)$ they are connected by equation (4.7) below (Kittel, 2005)

$$\sqrt{\mathcal{E}(\omega)} \equiv n(\omega) + iK(\omega) \qquad (4.7)$$

where $n(\omega)$ is the complex function of $\mathcal{E}(\omega)$.The refractive index, the extinction index and the reflectivity are related by equation (4.8) below (Kittel, 2005)

$$R(\omega) = \frac{n + iK - 1}{n + iK + 1} \qquad (4.8)$$

4.5 Structural Properties

The structural properties studied in this work were the lattice parameter, bond length, volume and the bond angle. The tetra potassium diarsenide zincate (K_4ZnAs_2) semiconductor compound has a trigonal crystal structure belonging to R-3m space group number 166 which crystallises into rhombohedral lattice with lattice parameters $a = b = 5.75$ Å, $c = 26.78$ Å which agrees very well with experimental work reported by Prots et. al., (2007) (Prots et al., 2007) . The mean lattice parameter from the six functionals was a = 18.2477 a. u., which is in good agreement with the experimental value of 18.2170 a. u. reported in the literature for the synthesised K4ZnAs2compound (Prots et al., 2007).

The crystal structure parameters including: the lattice a parameter, bulk modulus, equilibrium volume and enthalpy of formation energy were calculated by fitting the lattice parameter vs total energy, and cell volume vs total energy using the Birch-Murnaghan equation of state given by equation (4.9).

$$E(V) = E_o + \frac{B}{B'(B'-1)}\left[V\left(\frac{V_o}{V}\right)^{B'} - V_o\right] + \frac{B}{B'}(V - V_o) \qquad (4.9)$$

where in the equation above E_o, B, B′, V, and Vo are respectively, the optimum value of total energy, the bulk modulus, the pressure derivative of bulk modulus, the total unit cell volume, and the optimized unit cell volume.

4.5.1: K-Point Sampling

The k-points of the crystal structure were always placed in reciprocal spaces. When calculating the crystal structure, it is important to collect all periodic functions over the Brillouin zone. In the sampling of k-points, special k-point reciprocal spaces with high symmetry were selected for the calculation of other properties. The commonly known method used in the sampling of k-points is the Momkhorst-Pack method (Giannozzi et al.,2009). The Momkhorst-Pack method uses a spaced mesh in the Brillouin zone. The order used in the Momkhorst-Pack method is of the sequence (nd1 nd2 nd3 d1 d2 d3), where d1 d2 and d3 indicate the displacement of particles from the origin, a point where there is no offset. K-points are in an optimised state to give the optimised structure of the Brillouin zone for the calculated band structure.

In this study, we obtained the k-points from the material cloud website for use in the calculations of the band structure (Hinuma et al., 2017). Monkhorst-pack grids of 8 × 8 × 8, 9 × 9 × 9, and 8 × 8 × 8 for K_4ZnAs_2 were created as a result of convergence tests for k-points with energy.The positions along the high symmetrical axes were described $\boldsymbol{\Gamma}$, T, H2|H0, L, F SO|S2, F, Γ for K_4ZnAs_2 compound (R.Velavan1, Myvizhi.P2. (2018) . The summed energy as a function of unit volume and lattice constants was interpolated using the Murnaghan equation of state.The quantum espresso program was applied to calculate the elastic constants and other properties, such as bulk moduli, shear moduli, Young's moduli, and Poisson's ratio using three functions (Voigt, Reuss, and Hill's average). The hill averages of the bulk and shear moduli were used to compute the sound velocities. The Debye temperature was determined using a method that uses the angular averages of the sound velocity computed for each direction and solves the Kohn -Sham equation.

Then, was used to calculate the vibrational energy, constant strain heat capacity, free energy, and entropy within the Debye model (Tyuterev and Vast, 2006). The chosen k-path is specific to the material crystal structure obtained (Setyawan and Curtarolo, 2010). The density of states (DOS) was obtained from electronic structure calculations, and the k-points need to be dense as well (Sholl and Steckel, 2009).From the DOS, the material can be categorised as an insulator, semiconductor, or metal, and the band structure plot shows whether the bandgap is direct or indirect and the type of semiconductor material is.

4.5.2: Murnaghan Equation of States

The Murnaghan equation of states was used in this study to obtain the optimised volume, bulk modulus, and their respective derivatives. From a thermodynamic interpretation, an equation of states is related to the temperature, pressure, and volume of a crystal structure in the thermodynamic equilibrium state (Giannozzi et al.,2009). The relationship between the pressure and volume of a material with a constant number of particles is given by Equation (4.18) (Setyawan and Curtarolo,2010).

$$P(V) = \frac{B_0}{B_0^1}\left[\left(\frac{V_0}{V}\right)^{B_0^1} - I\right] \qquad (4.18)$$

To find the energy with respect to the volume, Equation (4.17) is integrated, leading to Equation (4.10).

$$\mathbf{E(V)} = \frac{\mathbf{B_0 V}}{\mathrm{B_0^1}}\left[\left(\frac{\mathbf{V_0}}{\mathbf{V}}\right)^{\mathrm{B_0^1}} \frac{\mathbf{1}}{\mathbf{B_0^1 - 1}} + \mathbf{I}\right] + \mathbf{Constant} \qquad (4.10)$$

where in the equation above E_o, B, B′, V, and Vo are respectively, the optimum value of total energy, the bulk modulus, the pressure derivative of bulk modulus, the total unit cell volume, and the optimized unit cell volume. In Q.E, the ev.x command file was applied by inputting the energy and volume values into the Murnaghan equation. This fitting was performed after lattice constant convergence was carried out wher the energies of different volumes were obtained.

4.5.3: Bulk Modulus and Its Pressure Derivative

In this study, the equilibrium bulk modulus and its respective pressure derivatives were generated by the application of the Murnaghan equation of states. The bulk modulus determines the resistance of the crystal structure to the compressive force acting on it. The volume and bulk modulus of a structure are inversely related to each other (Hung et al. 2018). The bulk modulus is given by equation (4.11)

$$B = -V\frac{\partial P}{\partial V} \tag{4.11}$$

Where B is the bulk modulus,V the volume and P is the pressure. The pressure of such system is given by equation (4.12) .

$$P = -\frac{\partial E}{\partial V} \tag{4.12}$$

When equation (4.12) is fitted into equation (4.11) then it reduces to equation (4.13) .

$$B = V\frac{\partial^2 E}{\partial V^2} \tag{4.13}$$

The derivative of pressure of the bulk modulus can be given by equation (4.23)

$$B' = \frac{\partial B}{\partial P} = \frac{1}{B}\left(V\frac{\partial}{\partial V}(V\frac{\partial^2 E}{\partial V^2})\right) \tag{4.23}$$

4.6: Electronic Properties

The electronic properties investigated in this study were the bandgap and density of states.

Electronic properties are crucial because they enable us to understand the manner in which the electrons of a material interact within the crystal structure and can be used to predict the general properties of a material (Hinuma et al., 2017). Band structure computations were performed using highly symmetrical points. Each symmetrical point is generated from a material project website (Hinuma et al., 2017).

4.7 Elastic Stability Analysis

The elastic constants are applied in the study of mechanical properties such as anisotropy, Young's modulus, bulk modulus, Poisson's ratio, and shear modulus of any material. DFT calculations use two methods to compute the elastic constants: the stress strain and energy strain methods. In this study, we used the stress-strain method to compute the elastic constants as per the Hooks law (Giannozzi et al., 2009).

The mechanical stability of the trigonal structure is given in equation (4.24) below.

$$\begin{cases} C_{11} > |C_{12}|, \ C_{44} > 0 \\ C_{13}^2 < \frac{1}{2} C_{33}(C_{11} + C_{12}) \\ C_{14}^2 < \frac{1}{2} C_{44}(C_{11} - C_{12}) \equiv C_{44} C_{66} \end{cases} \quad (4.24)$$

For any trigonal structure, the nine independent constants must satisfy Born stability criteria.

BV =

$$\frac{1}{9}[C_{11} + C_{22} + C_{33} + \frac{2}{9}[C_{12} + C_{13} + C_{23}] \quad (4.25)$$

The Bulk elastic properties (bulk modulus Bv, Young's modulus GR, and shear modulus G) were computed using the Voigt-Reuss-Hill schemes defined by equations (4.26) equation (4.30) (Fulfillment et al., 2021).

BR =1/

$$[(C_{11} + C_{22} + S_{33} + 2(C_{12} + C_{13} + C_{23})] \quad (4.26)$$

GR =15 /

$$[4(C_{11} + C_{22} + C_{33} - C_{12} - C_{12} - C_{23} + 3(C_{44} + C_{55} + C_{66})] \quad (4.27)$$

Where Si,j denotes the elastic compliance obtained by inverting the elastic constant matrix.

According to Hill approximation both bulk and shear modulus is defined by equation (4.28) and equation (4.28)

$$BH = \frac{1}{2}(B_R + B_V); \ G_H = \frac{1}{2}(G_R + G_V) \quad (4.28)$$

The Voigt bulk modulus BR and the Voigt shear modulus GR are defined by equation (4.29) and (4.30) respectively

$$BV = \frac{1}{9}\,[\,C11 + C22 + C33] + \frac{2}{9}\,[C12 + C13 + C23] \tag{4.29}$$

$$GR = \frac{1}{15}[C_{11} + C_{22} + C_{33} - C_{12} - C_{13} - C_{23} + \frac{1}{5}[C_{44} + C_{55} + C_{66}], \tag{4.30}$$

$$2(C_{14}^2 + C_{15}^2) < C44\ (C11 - C12) \tag{4.31}$$

The Poisson's ratio and Young's modulus are gotten from the shear and bulk moduli through the application of the equations (4.32) and (4.33), respectively (Dong et al., 2013; Hou, 2008).

$$\nu = \frac{3B_H - 2G_H}{2(3B_H + G_H)} \tag{4.32}$$

$$E_H = \frac{9B_H G_H}{(3B_H + G_H)} \tag{4.33}$$

The anisotropy in the interatomic binding energies in different matrices can be given by shear anisotropy.

The anisotropic factors A1 in the (100) planes between the < 011> and <010> directions, A2 in the {010} planes between the < 101> and <001> directions, and A3 in the {001} planes between the <110> and <010> directions are defined by equation (4.34) (Giannozziet al.).

$$A1 = \frac{4C_{44}}{C_{11} + C_{33} - 2C_{13}}\ ,\ \frac{4C_{55}}{C_{22} + C_{33} - 2C_{23}}\ ,\ \frac{4C_{66}}{C_{11} + C_{22} - 2C_{13}} \tag{4.34}$$

For any crystal structure of a compound with mechanical stability, strain energy must be greater than zero. This implies that the elastic stiffness must have the required inequalities, and Ci,j of different crystal structures must obey the specified conditions Dong et al., 2013; Hou, 2008).

CHAPTER FIVE: RESULTS AND DISCUSSIONS

5.0. Introduction

Results obtained from the studied properties (structural, electronic, elastin, mechanical and optical) of the trigonal Zintl phased tetra potassium diarsenido zincate (K_4ZnAs_2) semiconductor compound at the DFT theory level. Some of the experimental data for the K_4ZnAs_2 material like band gaps are known. The reason for this was to provide adequate insight into the K_4ZnAs_2 material. First, convergence tests including total energy, elat, cell energy, and k points are discussed, followed by the structural properties of the K_4ZnAs_2 material. (Giannozzi et al., 2009); (Mathematics, 2018) (Prots et al., 2007) are used as the main references.

5.1: Structural Properties

An ideal trigonal structure Zintl phased tetra potassium diarsenido zincate (K_4ZnAs_2) semiconductor compound e of belongs to the R3c space group. The unit cell is made up of 7 atomic particles, that is, 4 K atoms, 1 Zn atom and 2 As atoms. The visual appearance of the structure is shown in Figure 5.1 a. The structure of this material has two inequivalent K1+ sites, with the first K1+ site attached to three equivalent As3- atoms in a trigonal, non-coplanar geometry. In the first case, all K-As bond lengths are 3.47 Å. At the second K1+ site, K1+ is bound to four equivalent As3- atoms to form a mixture of edge- and corner-sharing K-As4 tetrahedra. There is one shorter (3.34 Å) and three longer (3.50 Å) K-As bond lengths. Zn2+ is bound to two equivalent As3- atoms in a linear geometry. Both Zn-As bond lengths are 2.33 Å. As3- is bound to seven K1+ and one Zn2+ atom in a distorted cubic cantering geometry. Distorted cubic cantering geometry (Sholl and Steckel, 2009).

Variable cell relaxation (vc relaxation) was performed on K4ZnAs2. The relaxed unit cell structure and the crystallographic data for a stable compound of K_4ZnAs_2 are a $= b = 5.78\text{Å}, c = 27.15\text{Å}, \alpha = \beta = 90°, = 120°, volume = 786.77\text{Å}^3$. Figure 5.1 b shows the lattice parameters of the relaxed unit cell structure of the K_4ZnAs_2.

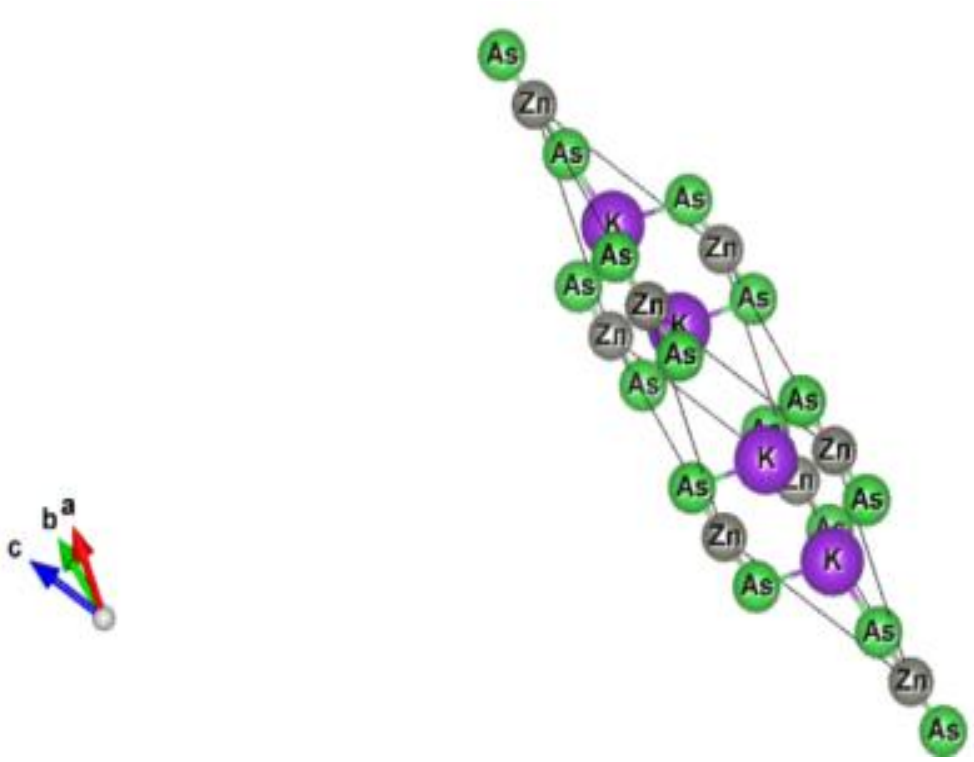

Figure 5.1: Structure of relaxed unit cell of the tetra potassium diarsenido zincate (K_4ZnAs_2).

The crystal system of the stable compound of K_4ZnAs_2 adopts a trigonal structure, and the lattice system is rhombohedra (Sholl and Steckel, 2009). The length of the unit cell as a function of energy was investigated, and it was realised that convergence was achieved for the tetra potassium diarsenido zincate (K_4ZnAs_2) semiconductor, as shown in Subsection (5.2.1).

5.2.1: Convergence Tests

K-point optimization using the six functionals, that is, PBE-GGA. PBEsol-GGA, LDA-PZ, BLYP-GGA, EVE-GGA, and SO-GGA were performed by moving from a 2 × 2 × 2 mesh to a denser mesh of 24 × 24 × 24, using an interval of 2 × 2 × 2. The converged K-points of the trigonal phase of the K4ZnAs2material using the six functionals were found to be 9 × 9 × 9, as shown in figures 5.2.1 (a)- (f). This mesh was selected to be optimum in this case; nevertheless, any value above it could be used. The higher the mesh, the denser the structure becomes, leading to more complicated computations, and is expensive even when the results obtained might be more accurate. This implies that the optimum mesh should be used to test convergence results (Giannozzi et al., 2009).

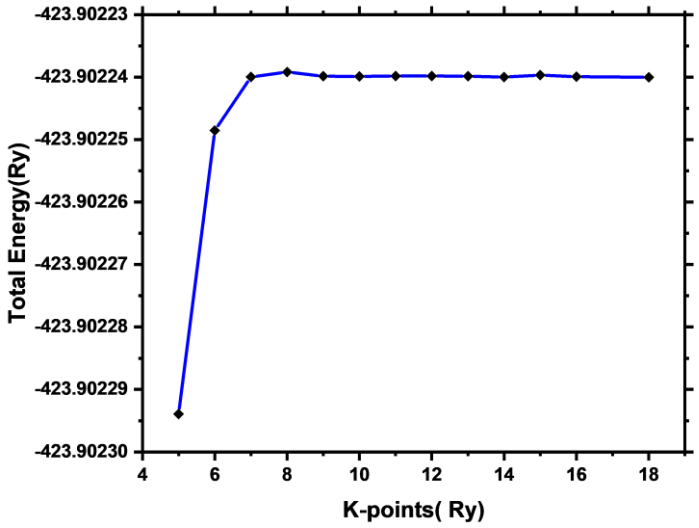

Figure 5.2 a BLYP

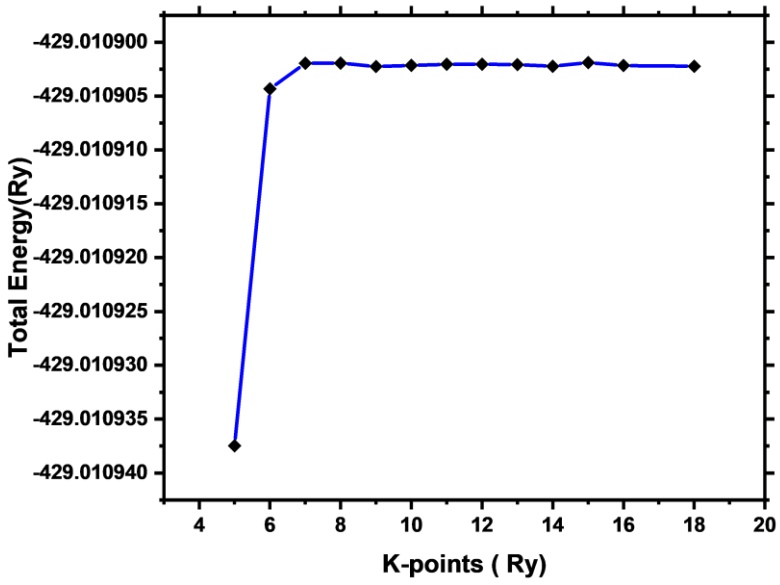

Figure 5.2 b EV

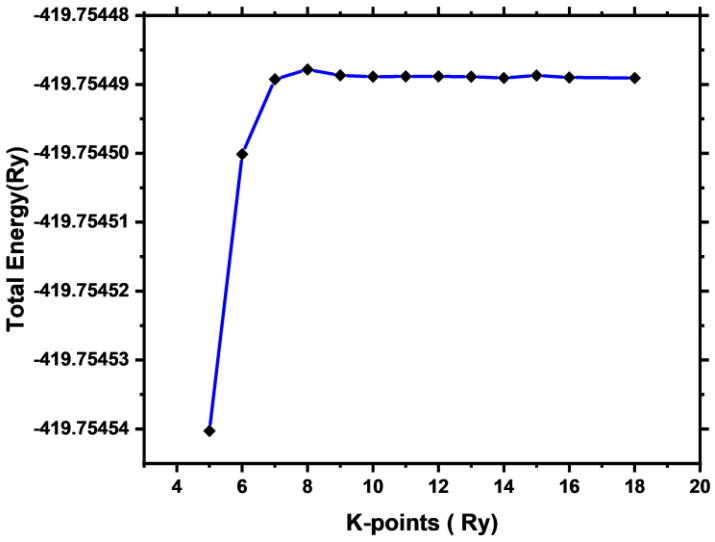

Figure 5.2.c LDA

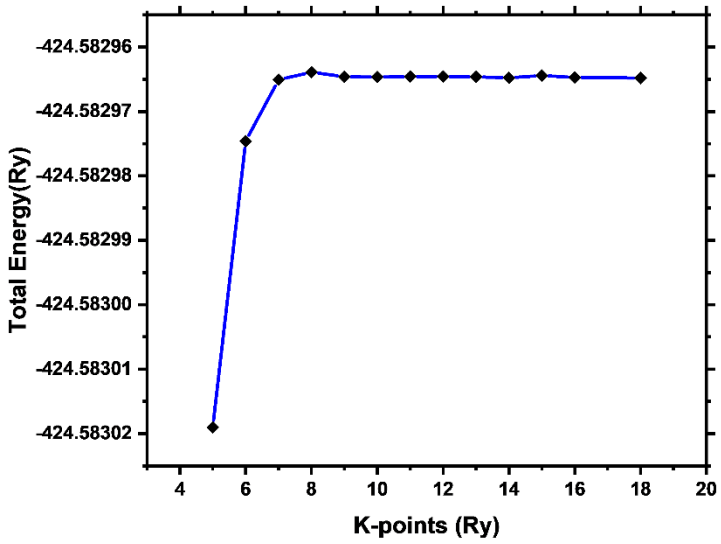

Figure 5.2 d PBE

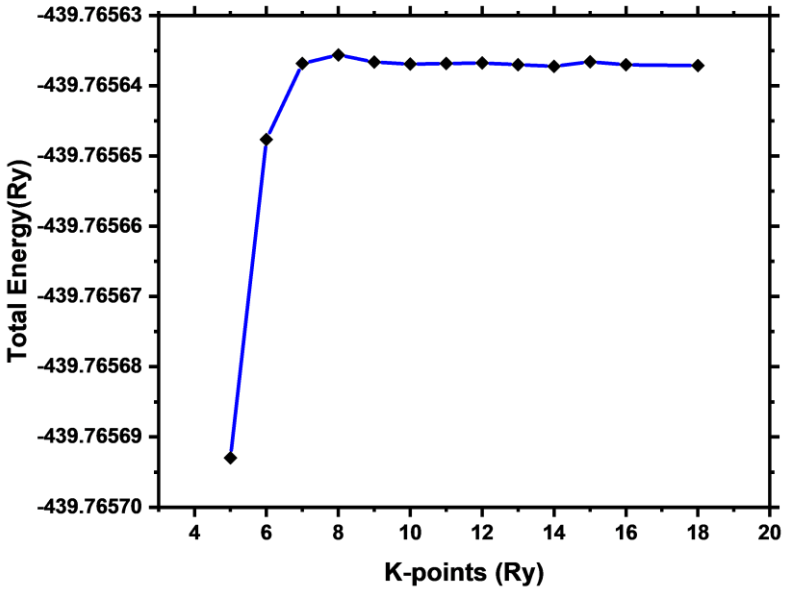

Figure 5.2 e PBEsol

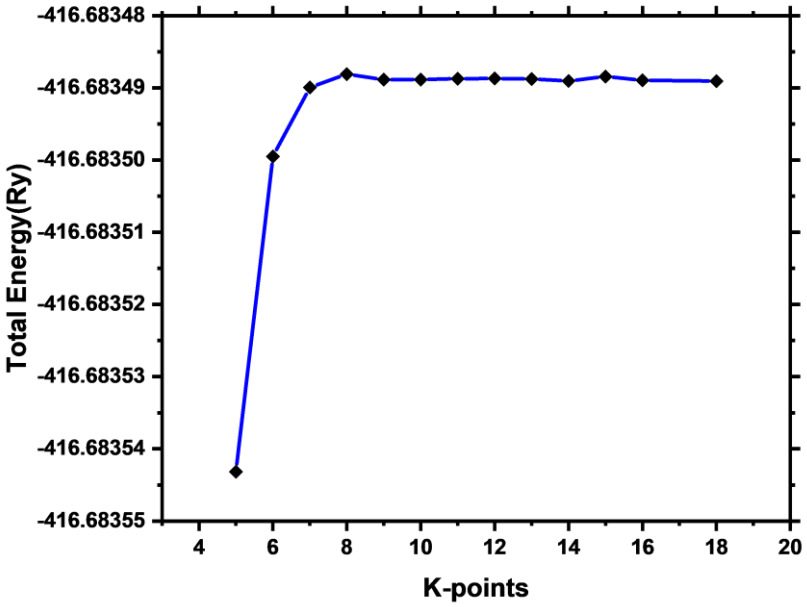

Figure 5.2 f SOGGA

Figure 5.2: k-point convergence for the tetra potassium diarsenido zincate (K_4ZnAs_2) semiconductor compound.

The optimised value of the converged mesh for the k-points, 9 × 9 × 9, was applied to test the convergence of the cutoff energy. Cutoff energy convergence was applied versus the energy in Ry.

Using the is PBE-GGA. PBEsol-GGA, LDA-PZ, BLYP-GGA, EVE-GGA and SO-GGA functionals for trigonal phase of K_4ZnAs_2 materials, the convergence tests were achieved at 120Ry as presented in the figure 5.2.2 (a-f).

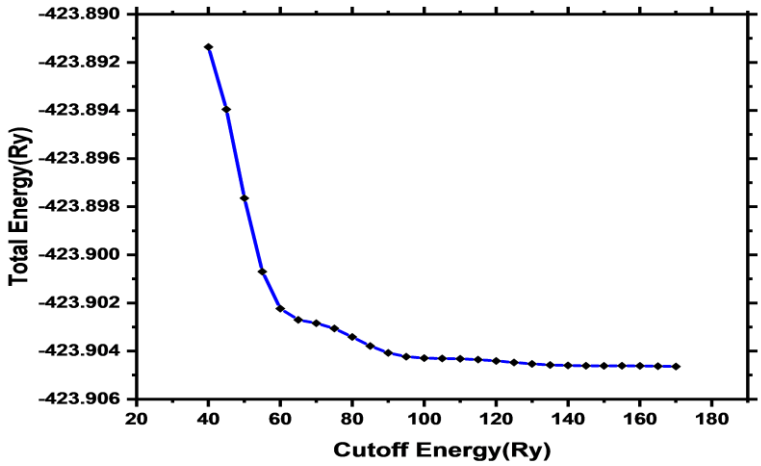

Figure 5.3 a BLYP

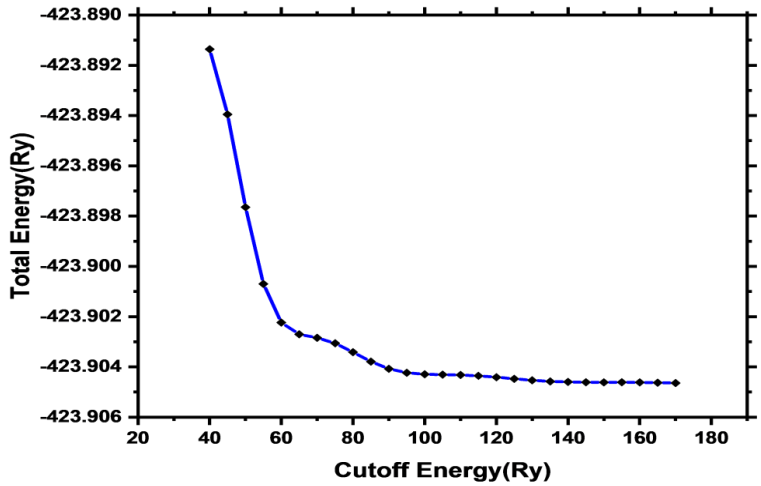

Figure 5.3 b EV

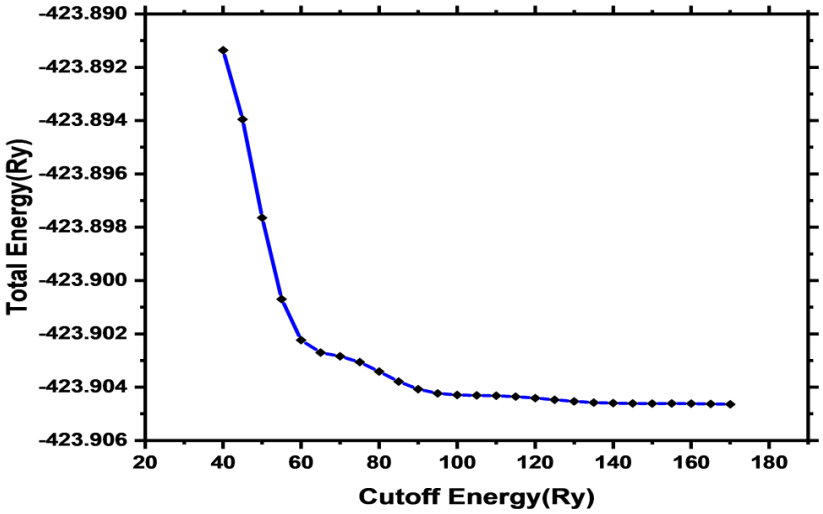

Figure 5.3 c LDA

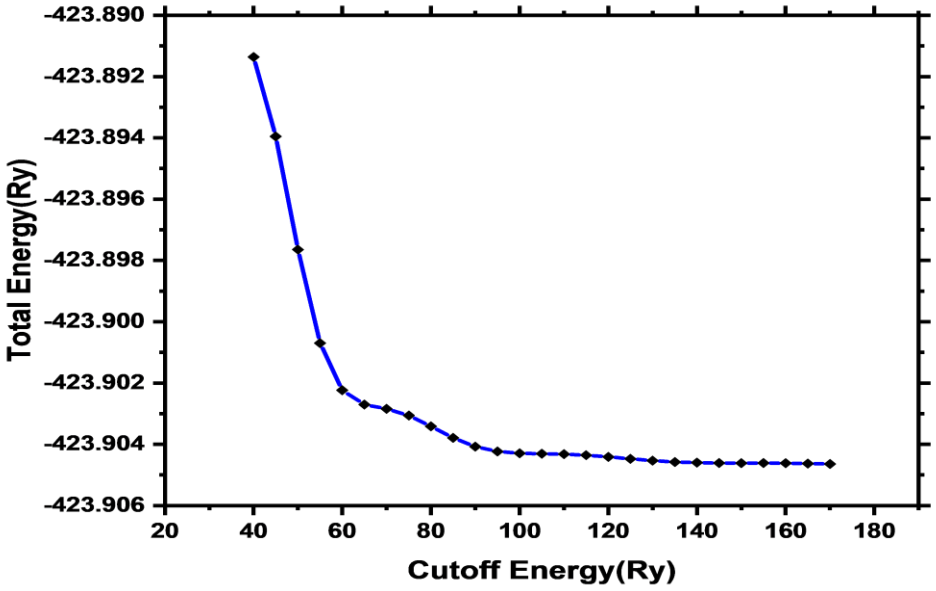

Figure 5.3 d PBE

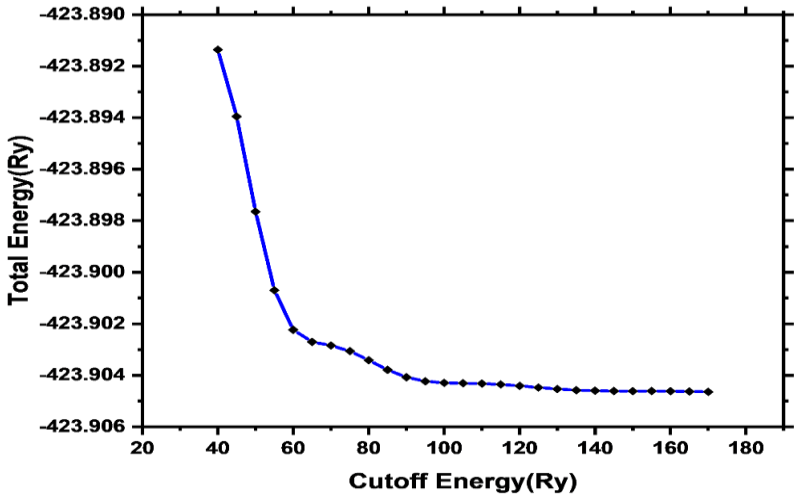

Fig 5.3 e PBEsol

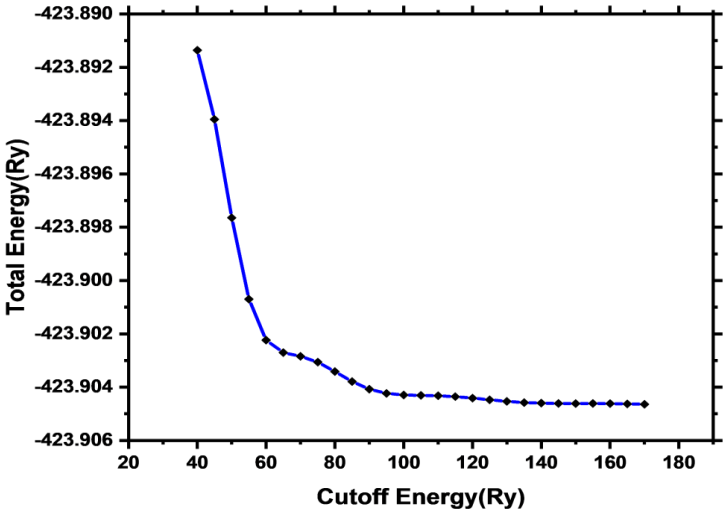

Fig 5.3 f SOGGA.

Figure 5.3.: Cutoff energy for the tetra potassium diarsenido zincate (K_4 $ZnAs_2$) semiconductor compound.

The cell dimension in the angle of the unit cell as a function of energy using eV was studied, and it was discovered that the convergence of the trigonal phase of K_4ZnAs_2 using six functionals, that is, PBE-GGA. PBEsol-GGA, LDA-PZ, BLYP-GGA, EVE-GGA, and SO-GGA methods were obtained.

The convergence of is PBE -GGA,PBEsol, LDA-PZ, BLYP-GGA, EVE-GGA and SO-GGA was achieved at 20.5Å, 20.5A, 17.25A, 18.25A, 18.25A and 17.25A respectively as shown in the figure 5.2.3 (a-f).

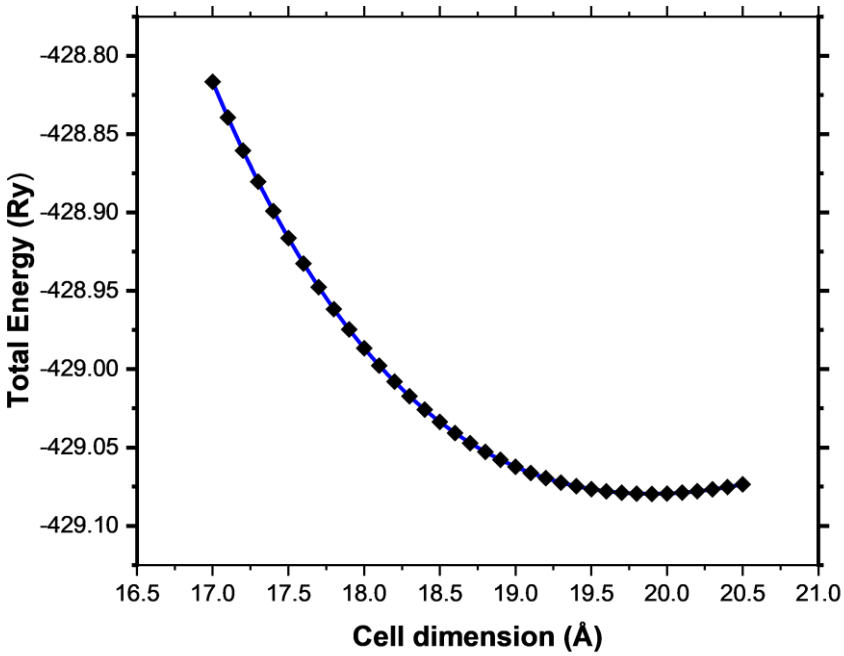

Fig 5.4 a BLYP.

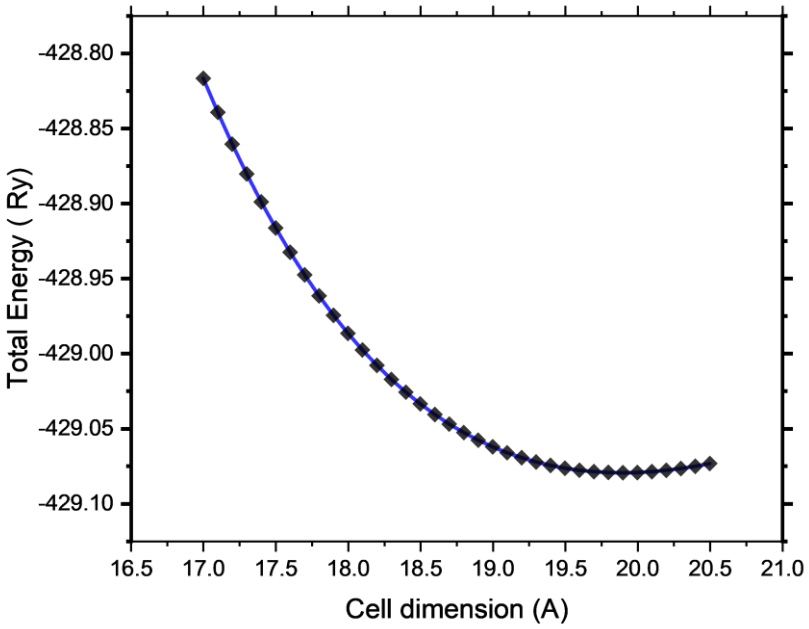

Fig 5.4 b EV.

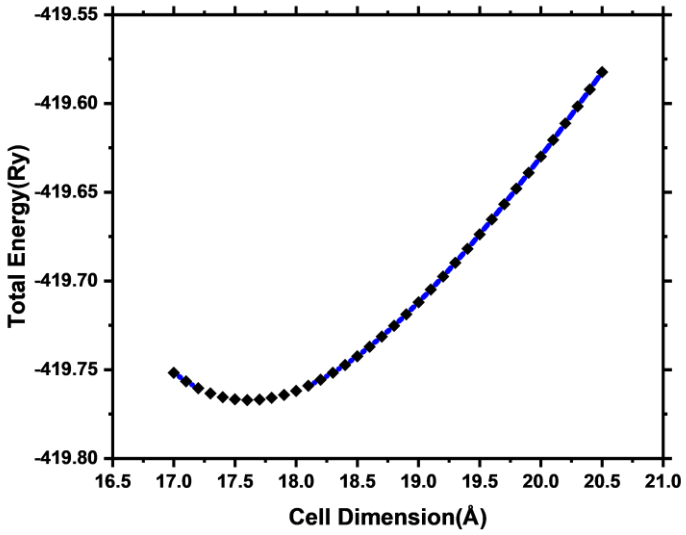

Fig 5.4 c LDA

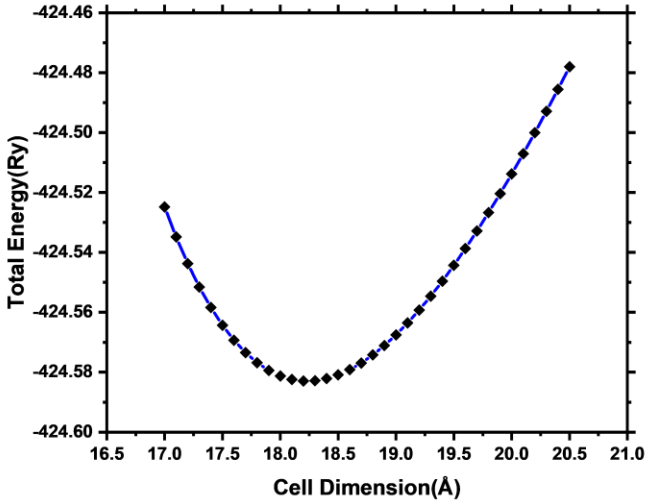

Fig 5.4 d PBE

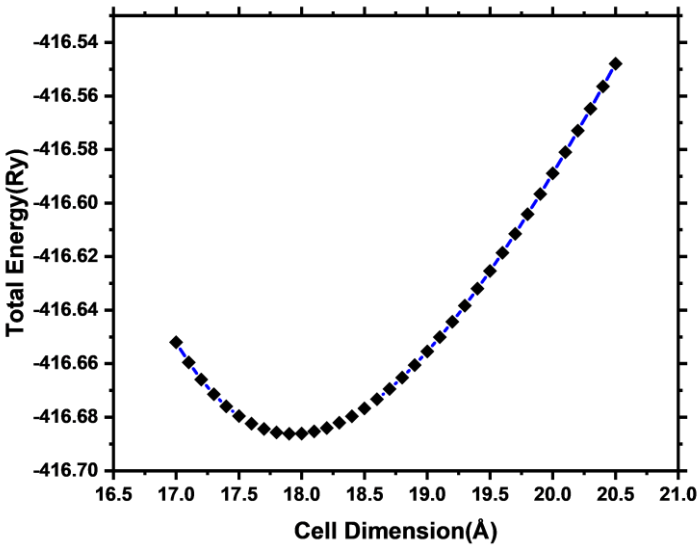

Fig 5.4 e PBEsol

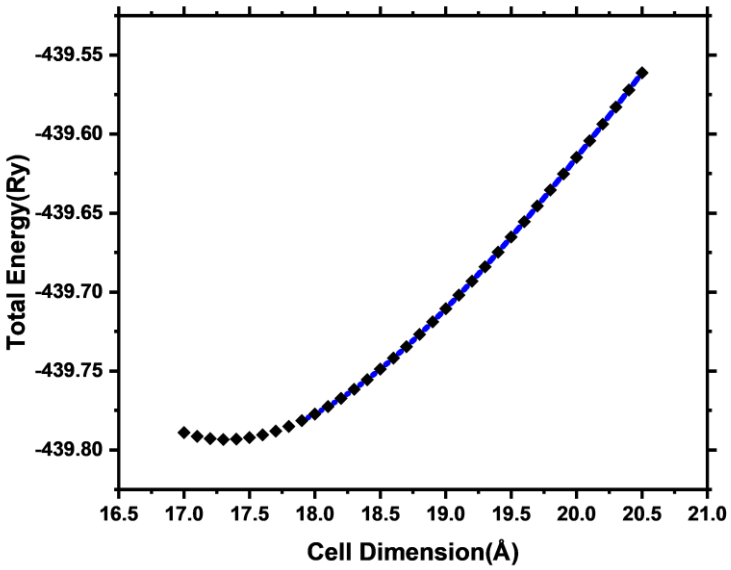

Fig 5.4 f SOGGA

Figure 5.4 **The cell dimensions convergence using eV in angstroms for tetra potassium diarsenido zincate (K_4ZnAs_2) semiconductor compound.**

The cell dimension in angstroms of the unit cell as a function of energy using elat convergence was studied and it was discovered that the convergence of the trigonal phase of K_4ZnAs_2 using the six functionals, that is PBE. PBEsol, LDA, BLYP, EVE, and SOGGA were not achieved.

The crystal structure parameters including: the lattice a parameter, bulk modulus, equilibrium volume and enthalpy of formation energy were calculated by fitting the lattice parameter vs total energy, and cell volume vs total energy using the Birch-Murnaghan equation of state of the tetra potassium diarsenido zincate (K_4ZnAs_2) semiconductor using six functionals, that is, PBE. PBEsol, LDA, BLYP, EVE, SOGGA and the results were as shown in table 5.1 below.

Table 5.1: Computed ground-state lattice parameters, bulk modulus, equilibrium volumes, and enthalpies of formation of K_4ZnAs_2 ternary compound using various correlation functionals.

	Lattice parameter ao (a.u)	**Bulk modulus Bo GPa**	**Equilibrium volume (a.u)3**	**Enthalpy of formation ΔHf (Ry)**
LDA	17.5986	7.2	5450.47	-419.77
PBE	18.2247	5.3	6053.12	-424.58
PBEsol	17.9182	6.0	5752.81	-416.69
BLYP	18.5201	4.7	6352.32	-423.90
EV	19.8910	3.2	7869.87	-429.09
SOGGA	17.3333	8.5	5207.72	-439.79
Experimental work	18.2170	-	-	-

From the table 5.1 above of the equation of states of the six functionals, the trigonal phase of the material is stable because it occupies the lowest Enthalpy of formation for the six functionals. Convergence was achieved because the value was less than 6 for all functionals. Because this material is energetically stable, it cannot be decomposed into any other structure under any given normal condition. Because the volume is also very low at the convergence point, we can conclude that as the symmetry deviates from the ideal structure, the volume continues to increase.

5.3 Electronic Properties

The optimum parameters obtained from the variable cell relaxation and lattice parameter optimization were used to calculate the electronic properties of the trigonal phase of tetra potassium diarsenido zincate (K_4ZnAs_2). To understand the electronic properties of the compound, ground state conditions were used to calculate the density of states, and the band structures of the trigonal phase of the tetra potassium diarsenido zincate (K_4ZnAs_2) structure were investigated along the symmetry points (Γ, T, H2|H0, L, F S0|S2, F, Γ) in the Brillouin zone using GGA-PBE, GGA-PBEsol, PZ-LDA, GGA-BLYP, GGA-EV, and GGA-SO as exchange-correlation functionals.

At the Fermi level EF (E=0), the material was noted to have an indirect band gap where the minima of the valence band were at the gamma point, while the maxima of the conduction band were at the F-symmetry point for all functionals used, confirming that K4ZnAs2is a semiconductor material. The electronic band structure indicates the band gap type of the material which is a crucial parameter that determines the type of application and suitability in optoelectronics. The obtained density of states and band diagrams for the tetra potassium diarsenido zincate (K_4ZnAs_2) trigonal structure for the GGA-PBE, GGA-PBEsol, PZ-LDA, GGA-BLYP, GGA-EV, and GGA-SO functionals are shown in Figures 5.5 (a-f).

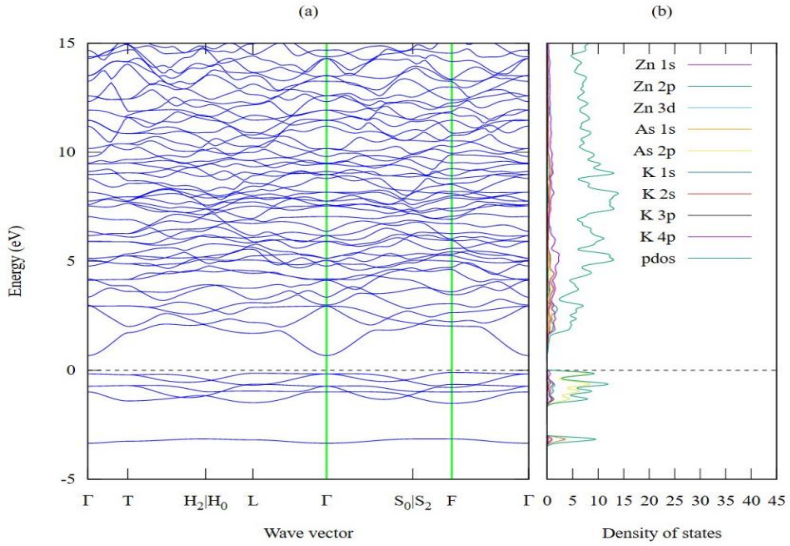

Fig 5.5 a BLYP

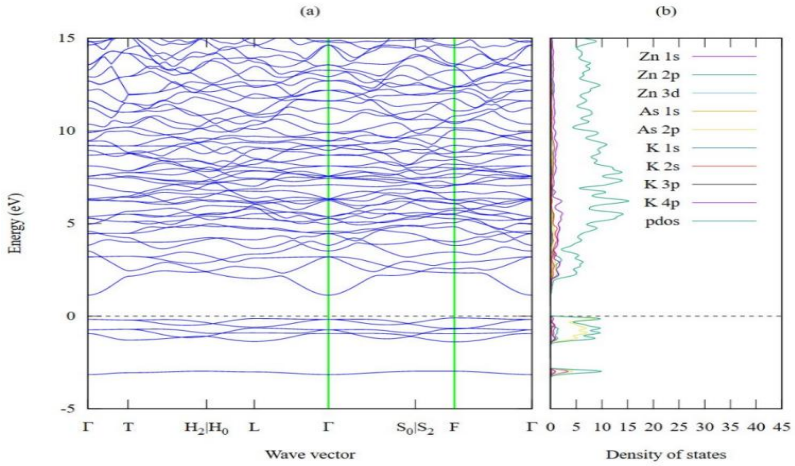

Fig 5.5 b EV

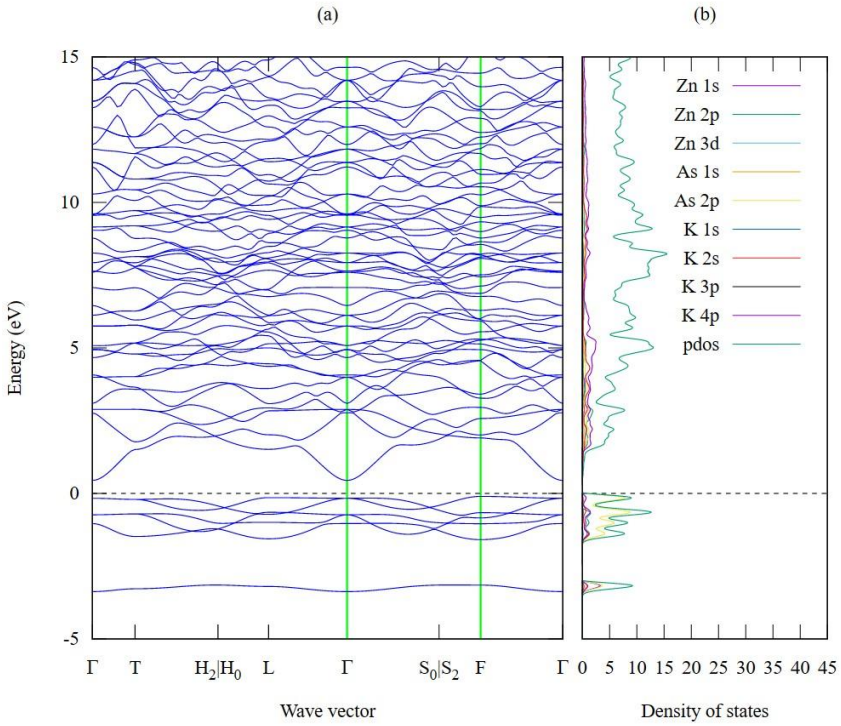

Fig 5.5 c LDA

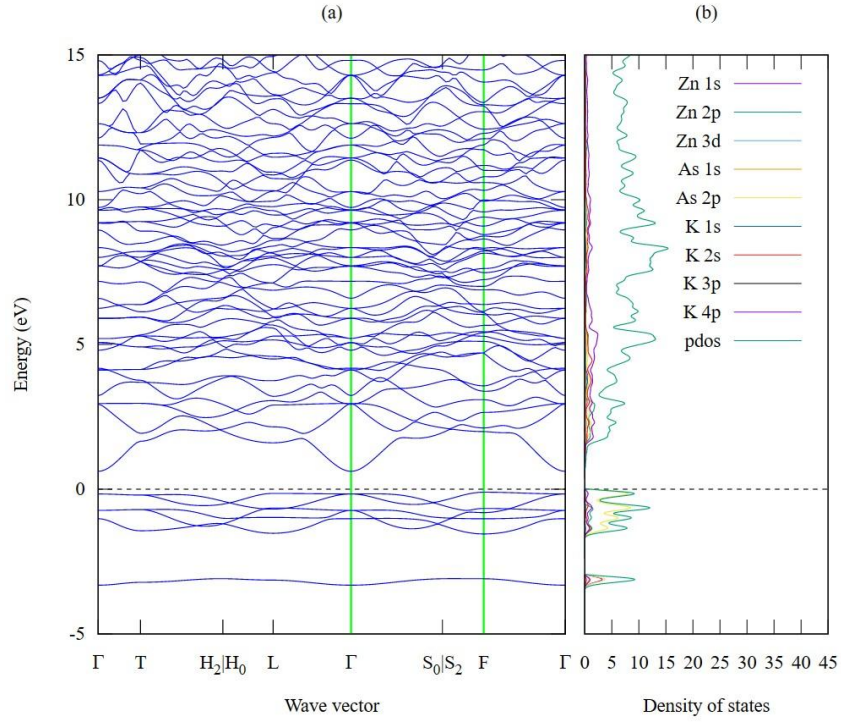

Fig 5. d PBE

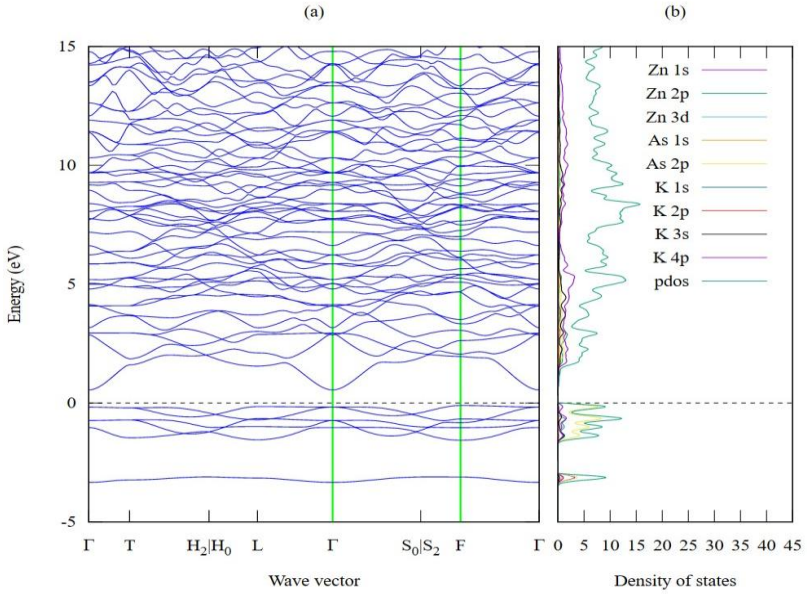

Fig 5.5 e PBEsol

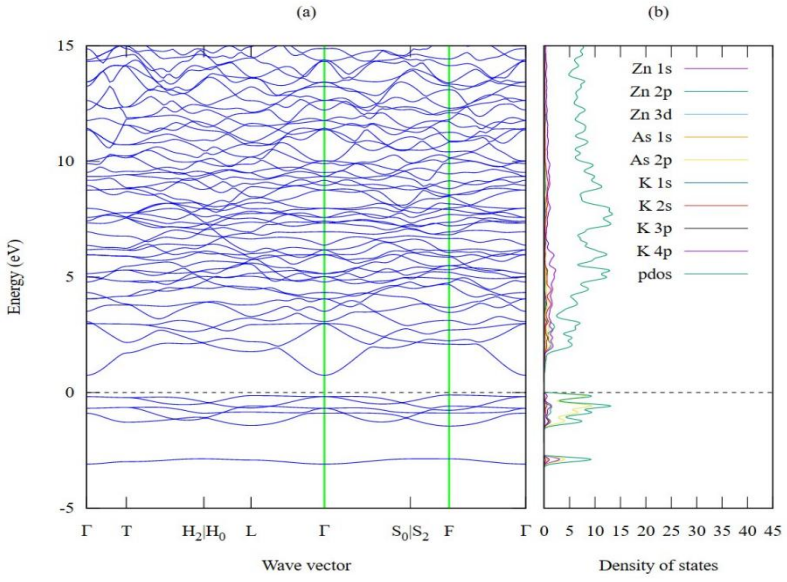

Fig 5.5 f SOGGA

***Figure 5.5*: The combined density of states and the wave vectors against energy in EV of the tetra potassium diarsenido zincate (K_4ZnAs_2).**

The smallest band gap (Eg =0.5493 eV) was obtained using LDA-PZ, which is known to underestimate the bandgap of materials, while the largest bandgap (Eg =1.2282 eV) was obtained using GGA-EV which has an advantage in predicting a good bandgap for semiconductor materials(Physics et al., 2020). The other functional predicted bandgaps of 0.7724 eV (GGA-BLYP), 0.7215 eV (GGA-PBE), 0.6565 eV (GGA-PBESol), and 0.8526 eV (SO-GGA). This study provides good insight into the bandgap of the material because of the use of a variety of functionals, each having its own intrinsic strength which sets it apart from the others. This material structure also exhibited no discontinuities throughout the chosen k-paths, as observed in Figure (5.5 a-f).

By calculating the density of states (DOS) of this material, we can determine the available electronic states/shell/orbitals that an electron can occupy so that a given atom can participate in the formation of a band-edge. The six functionals used in the analysis of the electronic properties of K4ZnAs2were as follows: the valence band was mainly dominated by the Zn-2p, Zn-3d, As-1s and As-2p orbitals, with very small contributions from other orbitals. The upper conduction band is mainly formed by K-4p, K-3p, K-1s, Zn-3d, Zn-2p, and Zn-1s orbitals, with little contribution from the other states. The dispersion characteristics of the conduction and valence bands indicated a strong interaction between the orbitals of the seven atoms of the K4ZnAs2structure. The interaction of the orbitals results in the hybridization of different states, leading to the formation of a band gap within the structure.

These interactions are essential for optoelectronic and photovoltaic applications, because they prevent optical transitions with the same electronic states to take place. This allows for maximum optical absorption of light energy in visible region.

5.4 Elastic and Mechanical Properties

The elastic properties are important for determining the structural, thermal, and mechanical stability of materials. Moreover, the elastic properties also provide information on how a material responds to both the intrinsic and extrinsic forces applied to its crystal structure. The elastic properties such as bulk modulus B, shear modulus G, Young's modulus E, and Poisson's ratio n, of Voigt approximation, Reuss approximation and the Voigt-Reuss-Hill approximation were computed in this study by using GGA-PBE. GGA-PBEsol, PZ-LDA, GGA-BLYP, GGA-EVE, and GGA-SO functionals as listed in Table 5.2(a-f).

Table 5. 2a: The bulk (B_V, B_R, B_H) and shear (G_V, G_R, G_H) moduli of the the tetra potassium diarsenido zincate (K_4ZnAs_2) materials in GPa under the Voight, Reuss and Hill averaging schemes calculated using the GGA-BLYP approximations.

	Bulk Modulus (B)	**Young Modulus (E)**	**Shear Modulus (G)**	**Poison ratio (n)**	$\frac{B}{G}$
Voigt Approximation	14.6649	20.7623	8.2127	0.26404	1.7856
Reuss - Approximation	14.4863	17.3634	6.6773	0.30022	2.1695
Voigt-Reuss-Hill Approximation	14.5756	19.0631	7.4450	0.28027	1.9578

Table 5. 2b: The bulk (B_V, B_R, B_H) and shear (G_V, G_R, G_H) moduli of the the tetra potassium diarsenido zincate (K_4ZnAs_2) materials in GPa under the Voight, Reuss and Hill averaging schemes calculated using the EV-GGA approximations.

	Bulk Modulus (B)	Young Modulus (E)	Shear Modulus (G)	Poison ratio (n)	$\frac{B}{G}$
Voigt Approximation	22.3265	23.3617	8.8117	0.32561	2.5337
Reuss - Approximation	22.1220	18.51616	6.8049	0.3649	3.2509
Voigt-Reuss-Hill Approximation	22.2237	20.9389	7.8083	0.34081	2.8462

Table 5. 2c: The bulk (B_V, B_R, B_H) and shear (G_V, G_R, G_H) moduli of the the tetra potassium diarsenido zincate (K_4ZnAs_2) materials in GPa under the Voight, Reuss and Hill averaging schemes calculated using the GGA-PBE approximations.

	Bulk Modulus (B)		**Shear Modulus (G)**	**Poison ratio (n)**	$\frac{B}{G}$
Voigt Approximation	15.033	21.029	8.2997	0.26685	1.8113
Reuss - Approximation	14.9110	17.3640	6.6481	0.3059	2.2429
Voigt-Reuss-Hill Approximation	14.9717	19.1964	7.4739	0.28422	2.0032

Table 5. 2 d: The bulk (B_V, B_R, B_H) and shear (G_V, G_R, G_H) moduli of the the tetra potassium diarsenido zincate (K_4ZnAs_2) material in GPa under the Voight, Reuss and Hill averaging schemes calculated using the SO-GGA, approximations.

	Bulk Modulus (B)	**Young Modulus (E)**	**Shear Modulus (G)**	**Poison ratio (n)**	$\frac{B}{G}$
Voigt Approximation	15.1570	21.5140	8.5140	0.26343	1.780
Reuss - Approximation	14.9749	17.9902	6.9205	0.29971	2.1638
Voigt-Reuss-Hill Approximation	15.0659	19.7620	7.7172	0.27973	1.9522

Table 5. 2 e: The bulk (B_V, B_R, B_H) and shear (G_V, G_R, G_H) moduli of the the tetra potassium diarsenido zincate (K_4ZnAs_2) materials in GPa under the Voight, Reuss and Hill averaging schemes calculated using the PZ-LDA approximations.

Approxination	Bulk Modulus (B)	Young Modulus (E)	Shear Modulus (G)	Poison ratio (n)	$\frac{B}{G}$
Voigt Approximation	13.3627	20.8280	8.3969	0.24022	1.5914
Reuss - Approximation	13.2412	17.3171	6.7538	0.28203	1.9606
Voigt-Reuss-Hill Approximation	13.3019	19.0725	7.5753	0.25886	1.7560

Table 5.2 f: The bulk (BV, BR, BH) and shear (GV, GR , GH) moduli of the the tetra potassium diarsenido zincate (K_4ZnAs_2) materials in GPa under the Voight, , Reuss and Hill averaging schemes calculated using the GGA-PBEsol approximations.

	Bulk Modulus (B)	Young Modulus (E)	Shear Modulus (G)	Poison ratio (n)	$\frac{B}{G}$
Voigt Approximation	15.1570	21.5137	8.5140	0.26342	1.7802
Reuss - Approximation	14.9749	17.9902	6.9205	0.29977	2.1638
Voigt-Reuss-Hill Approximation	15.0659	19.752	7.7173	0.27973	1.9522

The parameters used to define the mechanical properties, as shown in Table 5.2 (a-f), were consistently higher for the EV-GGA and SO-GGA functionals. The bulk modulus measures the resistance to the change in volume that occurs because of the external pressure applied to the material. The larger the value of the bulk modulus, the harder is the material. Based on the calculated bulk moduli using the six functionals, we predict that the the tetra potassium diarsenido zincate (K_4ZnAs_2) material is a soft material because, in all cases, the value of the bulk modulus is not very large, that is **B > 20** GPa (Giannozzi et al., 2009) . The ductility and brittleness of a material were determined using Pugh's (Giannozzi et al., 2009) and Poisson's ratio (Dong et al., 2013; Hou, 2008). A material is said to be brittle if the B/G ratio is less than 1.75, whereas if the material has a B/G ratio greater than 1.75, it implies that the material is ductile. The results obtained using these six functionals confirmed that the material is ductile.

Furthermore, the covalent or ionic properties of the material can be predicted using the Poisson's ratio n, for covalent material, the condition $\mathbf{0 < n < 0.25}$ is true, and ionic if $\mathbf{0.25 < n < 0.5}$ is true. Because the Poisson's ratios of the six functionals used were approximately greater than 0.25 and less than 0.5, this implies that the tetra potassium diarsenido zincate (K_4ZnAs_2) has ionic properties. These findings are in agreement with data in the literature (Dong et al., 2013).

Mechanical stability was obtained by confirming the elastic constants C_{ij} of the trigonal the tetra potassium diarsenido zincate (K_4ZnAs_2) structure using GGA-PBE. GGA-PBEsol, PZ-LDA, GGA-BLYP, GGA-EVE, and GGA-SO functionals. The tetra potassium diarsenido zincate (K_4ZnAs_2) ternary material adopts rhombohedral crystal structure belonging to Laue class $\bar{3}m$ featuring 7 independent elastic constants given as C11, C12, C13, C22, C33, C44, and C55 as shown in table 5.3 below. The most important and fundamental conditions for the elastic stability of rhombohedral lattice systems are given by Equation (4.24) in chapter four. The calculations show that trigonal the tetra potassium diarsenido zincate (K_4ZnAs_2) satisfies the necessary and sufficient conditions; therefore, the material is mechanically stable. (Giannozzi et al., 2009).

Table 5.3: The calculated elastic constants (C_{ij}) of the K4ZnAs2materials in GPa using GGA-PBE E V-GGA, SO-GGA, approximations.

Functional	**C11**	**C12**	**C13**	**C22**	**C23**	**C44**	**C55**
GGAPBE	27.462	9.5049	5.9807	27.4625	5.9807	4.4440	4.4340
EV-GGA	36.0311	16.0177	12.8158	36.0311	12.8158	4.3610	4.3610
SO-GGA	41.3018	20.2235	12.7362	41.3019	12.7362	5.2460	5.2460
BLYP-GGA	26.5477	8.8317	6.0032	26.5477	6.0032	4.5244	4.5244
GGA-PBEsol	27.4733	9.1858	6.1097	27.4713	6.1097	4.6807	4.6807
PZ-LDA	25.5825	7.5803	4.3027	25.5825	4.3027	4.5405	4.5405

Directional isotropy or anisotropy is the the directional dependency of the mechanical properties that is closely analogous to the plastic deformation and crack characteristics of a crystal structure. In this study, to get a comprehensive insight into the elastic isotropy/anisotropy of the tetra potassium diarsenido zincate (K_4ZnAs_2) Compound, the spatial dependencies of the Young's modulus, shear modulus, and Poisson's ratio were investigated, as shown in graphical representation in Figure (5.6 a-c).

(a)

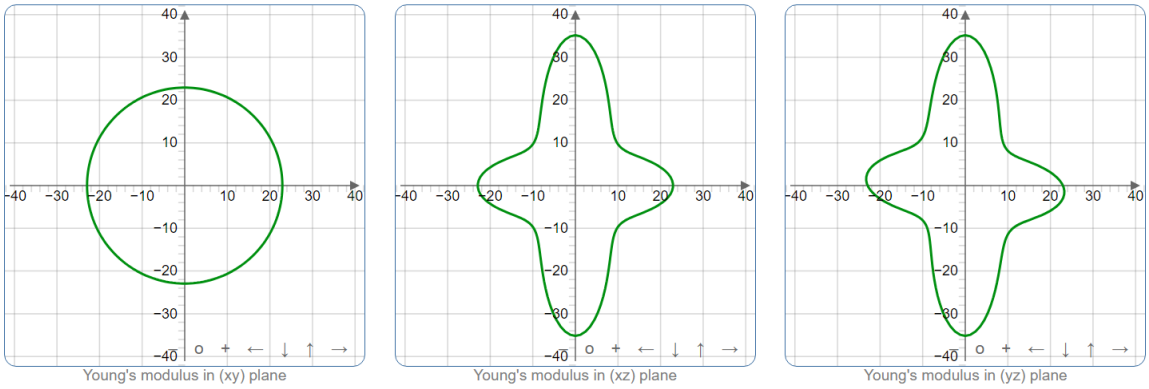

(b)

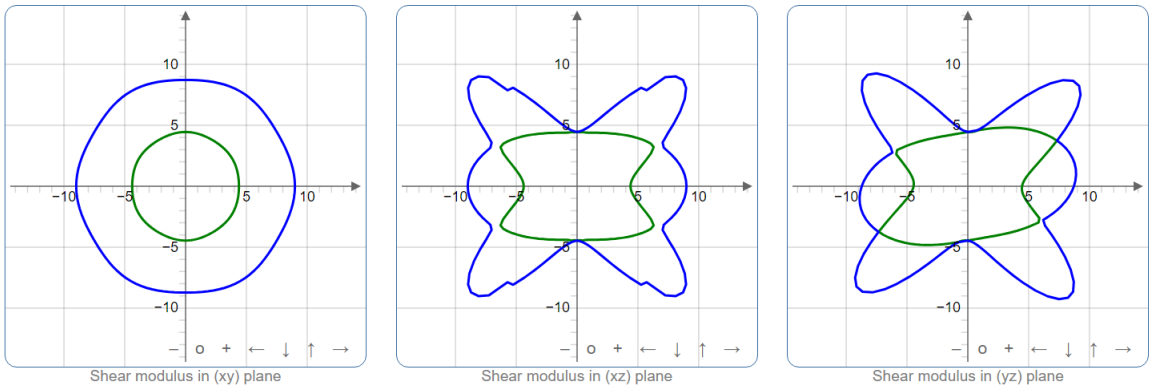

(c)

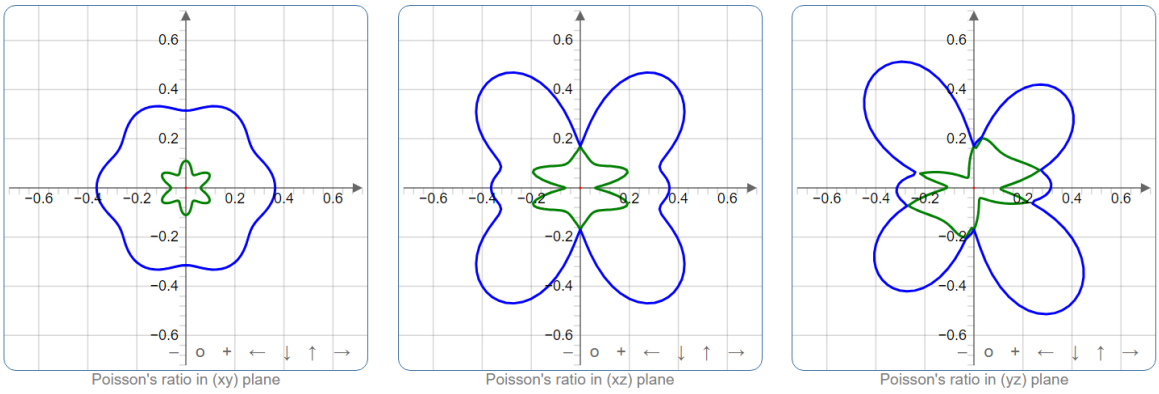

Figure 5.6: The spatial dependency of (a) Youngs modulus, (b) Shear modulus, and (c) Poisson's ratio

The degree of anisotropy is dependent on the deviation of a geometrical body from the spherical shape in this case, represented in a 2D shape. If a geometrical body is a spherical (3D) or circular (2D) shape, it exhibits isotropy, which is observed in the xy-plane for Young's modulus, shear modulus, and Poisson's ratio at varying degrees. It is also seen that for the xz-plane, the degree of anisotropy is slightly more symmetric for Young's modulus, shear modulus, and Poisson's ratio, while for the yz-plane, the anisotropy gives an antisymmetric distribution.

The anisotropic deviation from the computed values of Young's modulus were 12.749 GPa and 35.502 GPa for the minimum and maximum data, respectively, while the shear modulus and Poisson's ratio were 4.31 GPa,12.63 GPa and 0.045GPa 0.627GPa for the minimum and maximum data. This deviation displays an anisotropy values of 2.785, 2.929, and 13.8346 for the Young's modulus, shear modulus, and Poisson's ratio, respectively. The low data gotten here corroborate the earlier deduction that the material structure is ductile. In summary, the K2ZnAs2 compound displays isotropy in the xy-plane but anisotropy in the xz and yz planes.

5.5. Optical Properties

The optical properties of semiconductors are important because they determine how the material crystal structure interact with electromagnetic spectral radiation. This is the basis for technologies such as optical communication, displays, and optical storage. The optical properties depend on the band structure of semiconductors, which affects the optical permittivity and absorption coefficient, and their analysis can further extend our understanding of their suitability for optoelectronic and photovoltaic applications. In this study, crucial parameters were analysed to understand the suitability of this material. The results obtained for the optical properties are shown in Figure 4 (a-e).

The complex dielectric wave equation explains the response of the electrons of the material to the incident photon energy and is given by Equation (5.1).

$$\varepsilon(\omega) = \varepsilon_1(\omega) + \varepsilon_2(\omega) \qquad 5.1$$

where ε(ω) is the total angular frequency dependent dielectric function, $\varepsilon_1(\omega) = n^2 - k^2$ is the real part of the complex dielectric wavefunction with n and k being the refractive index and extinction coefficient respectively, and $\varepsilon_2(\omega) = 2nk$ is the imaginary part of the dielectric function. The $\varepsilon_1(\omega)$ defines the wave damping and energy dissipation, whereas the imaginary part $\varepsilon_2(\omega)$ is related to polarization and is responsible for the phonon absorption in a material.

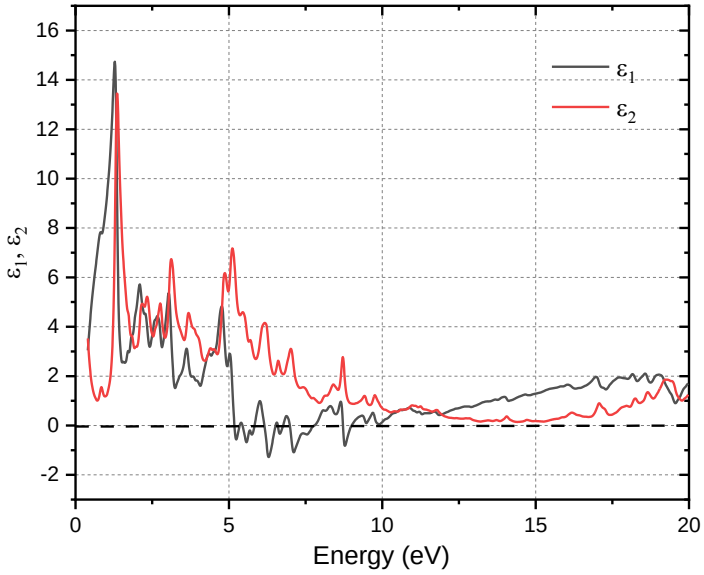

Figure 5.7 a: Dielectric constants epsilon 1 and epsilon 2 as a function of energy for the tetra potassium diarsenido zincate (K_4ZnAs_2).

The dielectric functions for this material showed that it was higher at lower energy from 1.0 eV to 7.0 eV and beyond there which dramatically decreases, indicating that the materials exhibit strong attenuation of the incident electromagnetic wave radiation within this region, and therefore exhibit metallic characteristics. The refractive index n(ω) and extinction coefficient k(ω) are important optical parameters for studying the potential applications of materials in optical and photonic devices. The expressions for the refractive index and extinction coefficients are given by Equations 5.2 and 5.6, respectively.

$$n(\omega) = \frac{1}{2}(\varepsilon_1(\omega) + (\varepsilon_1^2(\omega) + \varepsilon_2^2(\omega)^{1/2})^{1/2} \qquad 5.2$$

$$k(\omega) = \frac{1}{2}(-\varepsilon_1(\omega) + (\varepsilon_1^2(\omega) + \varepsilon_2^2(\omega)^{1/2})^{1/2} \qquad 5.3$$

Refractive index n (ω) is a useful parameter for predicting light refraction, particularly in optoelectronic applications. When photons come into contact with matter, they slow down owing to their interaction with electrons, and their refractive index is greater than one. However, if photons pass through a material with a higher refractive index n(ω), more photons are attenuated. There is a tendency for n (ω) to increase when the electronic density is increased.

The extinction coefficient k(ω) is analogous to ε2(ω), as observed in Figure 4a and 4b, and the dissimilarity of k(ω) from ε2(ω) is ascribed to the slight differences in optical conductivity [42]. In photonics, the extinction coefficient k(ω) is an important attribute of the fluorescence phenomenon; when the extinction coefficient is large, the fluorescence is proportionately high.

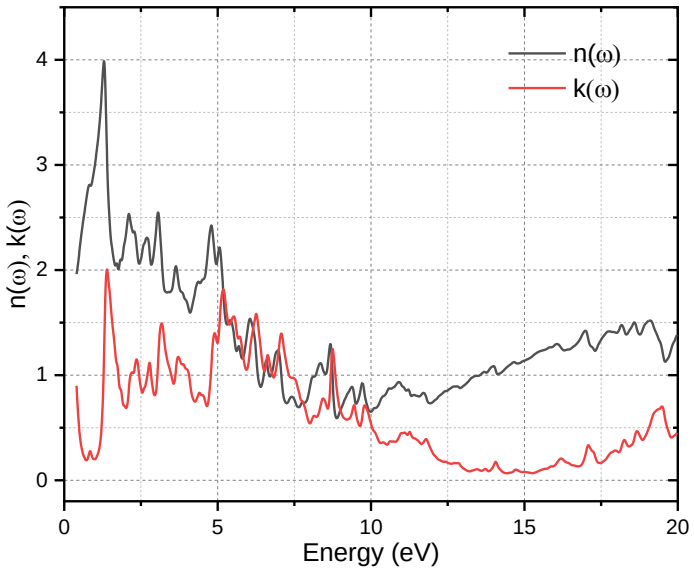

Figure 5.7 b: Refractive index and extinction coefficient as a function of energy for the tetra potassium diarsenido zincate (K_4ZnAs_2).

The other optical parameters used in this study are the absorption coefficient α , reflectivity R , and energy loss function L , as given in equations (5.4), (5.5), and used in Figures 5.7c, 5.7d, and 5.7e, respectively. The absorption coefficient measures the amount of light energy absorbed by a material. Reflectivity describes the surface characteristics of a material, while the energy-loss spectrum highlights the energy loss of electrons entering the material.

$$\alpha(\omega) = \sqrt{2}(\omega)\left(\sqrt{\varepsilon_1^2(\omega) + \varepsilon_2^2} - \varepsilon_1(\omega)\right)^{1/2} \quad 5.4$$

$$R(\omega) = \left(\frac{[n(\omega) - 1]^2 + k(\omega)^2}{[n(\omega) + 1]^2 + k(\omega)^2}\right) \quad 5.5$$

$$L(\omega) = \frac{\varepsilon_2(\omega)}{\varepsilon_1^2(\omega) + \varepsilon_2^2(\omega)} \quad 5.6$$

The absorption coefficient is an important parameter which is closely related to the skin depth of the material in which the electromagnetic wares interact with. Figure 4c shows a graphical representation of the calculated absorption coefficient of the tetra potassium diarsenido zincate (K_4ZnAs_2) compound which spans from the deep ultraviolet region at 20 eV to the infrared region. The wide absorption range of this material is an important characteristic desirable for applications in the optoelectronic and photovoltaic industries. The absorption spectra $\alpha(\omega)$ can be used to explain the case of absorption of the incident photon energy. It measures the quantity of light energy absorbed by the material. The computed spectra of $\alpha(\omega)$ for the tetra potassium diarsenido zincate (K_4ZnAs_2) are presented in Figure 4c. In the spectra of $\alpha(\omega)$, it is shown that initially the value of $\alpha(\omega)$ is zero, and the peaks start appearing from around 0.71eV which corroborates earlier values obtained for the electronic bandgap. The absorption spectrum of the tetra potassium diarsenido zincate (K_4ZnAs_2) had a wide range of 1.5 - 14.5 eV spanning the UV-Vis range and again at 16 eV – 20 eV.

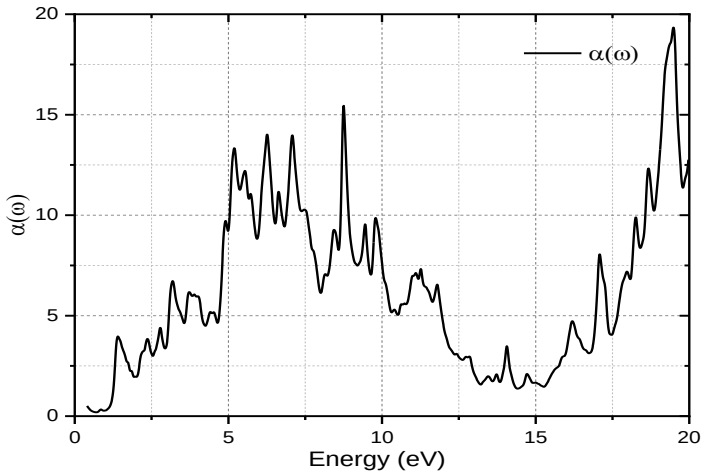

Figure 5.7 c: Absorption coefficient as a function of energy for the tetra potassium diarsenido zincate (K_4ZnAs_2).

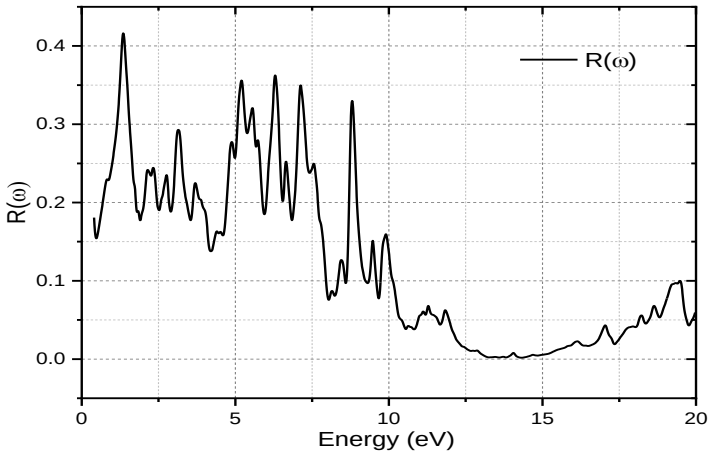

Figure 5.7 d: Reflectivity as a function of energy for the tetra potassium diarsenido zincate (K_4ZnAs_2).

The optical surface properties of a material are best described using reflectivity characteristics. In Figure (5.7 d), the reflectivity of the the tetra potassium diarsenido zincate (K_4ZnAs_2) compound is highest between 0 eV and 11 eV, which corroborates the observation of the absorption coefficient in Figure 4c as well as the energy loss function, as shown in Figure (5,7e).

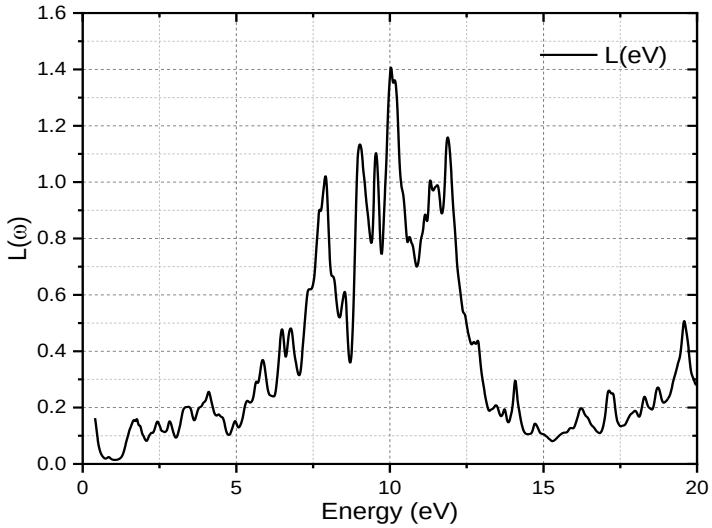

Figure 5.7 e: Energy loss function as a function of energy for the tetra potassium diarsenido zincate (K_4ZnAs_2).

Major energy loss peaks were observed in the slightly higher region of approximately 7 -13 eV. No energy loss peaks were observed in the visible region. No significant peaks were observed in the visible region.

CHAPTER SIX: CONCLUSIONS AND RECOMMENDATIONS

6.1: Introduction

This chapter presents the conclusions drawn from the results and work that remains to be done.

6.2: Conclusions

The structural, electronic, mechanical, elastic, and optical properties of trigonal K4ZnAs2ternary pnictide structures were studied using the first-principles method with triangulation of six exchange correlation functionals: LDA-PZ, GGA-PBE, GGA-PBESol, GGA-EV, GGA-BLYP, and SO-GGA. The material has been predicted to be mechanically stable, with bandgaps ranging between 0.5493 and 1.2282 eV. The most important and fundamental conditions for the elastic stability of rhombohedral lattice was satisfied. The lattice parameter and bandgap values were in agreement with previous experimental and theoretical studies, respectively. The conduction band formation was found to be mainly due to Zn 1s and Zn 2p, with low contributions from the As 2p and K 2s orbitals, and the other orbitals making insignificant contributions. On the other hand, the valence band formation is mainly due to the As 2p orbital, with some significant contributions from Zn 2p, Zn 1s, and K 2s, and other orbitals making minor contributions. The results revealed that K4ZnAs2absorbs light energy within the UV-VIS region of the electromagnetic spectrum as well as in the infrared region, showing excellent potential for optoelectronic and photovoltaic applications.

6.3: Recommendations

Studying the optical, elastic, structural, and electronic properties is of great importance when studying material applications, such as photovoltaics and other optoelectronic applications. For the band gap calculation, the six-exchange correlational functional used in this work normally underestimated while others overestimate the band gap energy especially when investigating a single phase. Work still needs to be done to investigate this material in different phases, such as monoclinic and tetragonal phases, for more accurate band gap precision. We also recommend band gap engineering studies to be carried out so as to tune the band gaps for optoelectronic applications.

We also recommend that other stoichiometries of the K4ZnAs2material be studied with the inclusion of double, triple, and mixed phases. We suggest that this material be investigated using other functionals such as local density approximation + Coulomb interaction (LDA+U) and generalised gradient approximation + Coulomb interaction (GGA+U) using various suitable pseudo-potentials. In addition to photovoltaics and optoelectronic applications, we recommend that investigations be done on this material so that it may be considered for other applications.

REFERENCES

1. AJain ,“Commentary: The Materials Project: A materials genome approach to accelerating materials innovation,” APL Mater, vol. 1, no. 1, p. 011002, Jul. 2013, doi: 10.1063/1.4812323.
2. Bartolotti, L. J. and Flurchick, K. (2007). An Introduction to Density Functional Theory. Reviews in Computational Chemistry, 7, 187–216. https://doi.org/10.1002/9780470125847.ch4
3. Berends, A. C., Mangnus, M. J. J., Xia, C., Rabouw, F. T., and De Mello Donega, C. (2019). Optoelectronic Properties of Ternary I-III-VI 2 Semiconductor Nanocrystals: Bright Prospects with Elusive Origins. Journal of Physical Chemistry Letters, 10(7), 2–8. https://doi.org/10.1021/acs.jpclett.8b03653.
4. BMiehlich, A. Savin, H. Stoll, and H. Preuss, “Results obtained with the correlation energy density functionals of becke and Lee, Yang and Parr,” Chem Phys Lett, vol. 157, no. 3, pp. 200–206, May 1989, doi: 10.1016/0009-2614(89)87234-3.
5. Bretonnet, J. L. (2017). Basics of the density functional theory. AIMS Materials Science, 4(6), 1372–1405. https://doi.org/10.3934/MATERSCI.2017.6.1372
6. Burke, K. (2007). http://chem.ps.uci.edu/˜kieron/dft/book/ The ABC of DFT. 1(2007), 84–122.
7. Burke, K., Perdew, J. P., and Ernzerhof, M. (1997). Why the generalized gradient approximation works and how to go beyond it. International Journal of Quantum Chemistry, 61(2), 287–293. https://doi.org/10.1002/(SICI)1097-461X(1997)61:2<287::AID-QUA11>3.0.CO;2-9
8. Callow, T. J., Hansen, S. B., Kraisler, E., and Cangi, A. (2021). First-principles derivation and properties of density-functional average-atom models. 1(5), 1–28. http://arxiv.org/abs/2103.09928
9. Dong, H., Chen, C., Wang, S., Duan, W., and Li, J. (2013). Elastic properties of tetragonal BiFeO3 from first-principles calculations. Applied Physics Letters, 102(18). https://doi.org/10.1063/1.4804641.
10. Dorado, B., Amadon, B., Freyss, M., and Bertolus, M. (2009). ioxidDFT + U calculations of the ground state and metastable states of uranium de. 1–8. https://doi.org/10.1103/PhysRevB.79.235125
11. Elenewski, J. E., and Hackett, J. C. (2012). A GGA + U approach to effective electronic correlations in thiolate-ligated iron-oxo (IV) porphyrin. Journal of Chemical Physics, 137(12), 1–10. https://doi.org/10.1063/1.4755290

12. Faculty, T. A., and Fulfillment, I. P. (2006). First-principles Calculations on the Electronic, Vibrational , and Optical Properties of Semiconductor Nanowires First-principles Calculations on the Electronic , Vibrational , and Optical Properties of Semiconductor Nanowires. Chemistry and Biochemistry, 1(December), 15–17.
13. Fan, Q., Zhang, W., Qing, H., and Yang, J. (2022). Exceptional Thermoelectric Properties of Bilayer GeSe: First Principles Calculation. Materials, 15(3), 1–11. https://doi.org/10.3390/ma15030971
14. Fulfillment, I. P., Putatunda, A., and Supervisor, T. (2021). FIRST-PRINCIPLES INVESTIGATION OF TRANSPORT AND MAGNETISM. 2(May), 2–7.
15. Giannozzi, P., Baroni, S., Bonini, N., Calandra, M., Car, R., Cavazzoni, C., Ceresoli, D., Chiarotti, G. L., Cococcioni, M., Dabo, I., Corso, A. D., Fratesi, G., Gironcoli, S. De, Gebauer, R., Gerstmann, U., Gougoussis, C., Kokalj, A., Martin-samos, L., Marzari, N., … Wentzcovitch, R. M. (2009). Q UANTUM ESPRESSO : a modular and open-source software project for quantum simulations of materials. Condensed Natter Physsics, 21(39),(2009), 395502–39505.
16. Golesorkhtabar, R., and Pavone, P. (n.d.). ElaStic : A universal tool for calculating elastic constants from first principles.
17. Harrison, N. M. (n.d.). An Introduction to Density Functional Theory.
18. Hinuma, Y., Pizzi, G., Kumagai, Y., Oba, F., and Tanaka, I. (2017). Band structure diagram paths based on crystallography. Computational Materials Science, 128, 140–184. https://doi.org/10.1016/J.COMMATSCI.2016.10.015.
19. Idrissi, S., Labrim, H., Bahmad, L., and Benyoussef, A. (2021). DFT and TDDFT studies of the new inorganic perovskite CsPbI3 for solar cell applications. Chemical Physics Letters, 766(January), 138347. https://doi.org/10.1016/j.cplett.2021.138347.
20. Irfan, M., Azam, S., and Iqbal, A. (2021). Proposal of new stable ABC2 type ternary semiconductor pnictides K3Cu3P2 and K3Ni3P2: First-principles calculations and prospects for thermosphysical and optoelectronic applications. International Journal of Energy Research, 45(2), 2980–2996. https://doi.org/10.1002/er.5992
21. Jaffe, J. E., and Zunger, A. (1984). Electronic structure of the ternary pnictide semiconductors ZnSiP2, ZnGeP2, ZnSnP2, ZnSiAs2, and MgSiP2. Physical Review B, 30(2), 1. https://doi.org/10.1103/PhysRevB.30.741
22. Javey, A. (2006). Microfabrication Technology Introduction to Materials Evolution of Devices. 1, 1(2006), 5.
23. Jeong, B., Jeong, M., Song, Y., Park, K., and Park, J. (2021). Screening of II-IV-V 2 Materials for Photovoltaic Applications.

24. Kopacic, I., Friesenbichler, B., Hoefler, S. F., Kunert, B., Plank, H., Rath, T., and Trimmel, G. (2018). Enhanced Performance of Germanium Halide Perovskite Solar Cells through Compositional Engineering. ACS Applied Energy Materials, 1(2), 343–347. https://doi.org/10.1021/acsaem.8b00007.
25. Liu, Q. J., Qin, H., Jiao, Z., Liu, F. S., and Liu, Z. T. (2016). First-principles calculations of structural, elastic, and electronic properties of trigonal ZnSnO3 under pressure. Materials Chemistry and Physics, 180, 75–81. https://doi.org/10.1016/j.matchemphys.2016.05.041.
26. Liu, X., Yang, Z., Chueh, C. C., Rajagopal, A., Williams, S. T., Sun, Y., and Jen, A. K. Y. (2016). Improved efficiency and stability of Pb-Sn binary perovskite solar cells by Cs substitution. Journal of Materials Chemistry A, 4(46), 17939–17945. https://doi.org/10.1039/c6ta07712a.
27. Körbel, S., Marques, M. A. L., and Botti, S. (2016). Stability and electronic properties of new inorganic perovskites from high-throughput: Ab initio calculations. Journal of Materials Chemistry C, 4(15), 3157–3167. https://doi.org/10.1039/c5tc04172d.
28. Malakkal, L., Szpunar, B., Zuniga, J. C., Siripurapu, R. K., and Szpunar, J. A. (2016). First principles calculation of thermo-mechanical properties of thoria using Quantum ESPRESSO. International Journal of Computational Materials Science and Engineering, 5(2), 1–15. https://doi.org/10.1142/S2047684116500081.
29. Mohamed Mansour, E. (2020). Equation of State. In Inverse Heat Conduction and Heat Exchangers. IntechOpen. https://doi.org/10.5772/intechopen.89919
30. H. J. Monkhorst and J. D. Pack, “Special points for Brillouin-zone integrations,” Phys Rev B, vol. 13, no. 12, pp. 5188–5192, Jun. 1976, doi: 10.1103/PhysRevB.13.5188.
31. Mathematics, A. (2018). " Influence of Individual Atoms in Binary and Ternary Semiconductors ". 119(12), 7263–7276.
32. Mbilo, M., Manyali, G. S., Musembi, R. J., Ar-, G., and Ge, S. (2022). Ab Initio Study of K 3 Cu 3 P 2 Material for Photovoltaic Applications. 1(2022), 1–6.
33. Mouhat and F.-X. Coudert, “Necessary and sufficient elastic stability conditions in various crystal systems,” Phys Rev B, vol. 90, no. 22, p. 224104, Dec. 2014, doi: 10.1103/PhysRevB.90.224104.
34. Naher, M. I., and Naqib, S. (2022). First-Principles Insights into the Mechanical, Optoelectronic, Thermophysical, and Lattice Dynamical Properties of Binary Topological Semimetal Baga2. SSRN Electronic Journal, 4(2022), 1–35. https://doi.org/10.2139/ssrn .4033392

35. Omata, T., Nagatani, H., Suzuki, I., and Kita, M. (2015). Wurtzite-derived ternary I-III-O2 semiconductors. Science and Technology of Advanced Materials, 16(2), 24902. https://doi.org/10.1088/1468-6996/16/2/024902
36. Ou, X., Chen, X., Xu, X., Xie, L., Chen, X., Hong, Z., Bai, H., Liu, X., Chen, Q., Li, L., and Yang, H. (2021). Recent Development in X-Ray Imaging Technology: Future and Challenges. Research, 2021(1), 1–18. https://doi.org/10.34133/2021/9892152
37. Perdew and A. Zunger, "Self-interaction correction to density-functional approximations for many-electron systems," Phys Rev B, vol. 23, no. 10, pp. 5048–5079, May 1981, doi: 10.1103/PhysRevB.23.5048.
38. Physics, S., Notes, L., and Rademaker, L. (2020). A Practical Introduction to Density Functional Theory. 1(2020), 1–22.
39. Prots, Y., Aydemir, U., Öztürk, S. S., and Somer, M. (2007). Crystal structure of tetrapotassium diarsenidozincate, the tetra potassium diarsenido zincate (K_4ZnAs_2). Zeitschrift Fur Kristallographie - New Crystal Structures, 222(3), 163–164. https://doi.org/10.1524/ncrs.2007.0067
40. Ziesche, S. Kurth, and J. P. Perdew, "Density functionals from LDA to GGA," Comput Mater Sci, vol. 11, no. 2, pp. 122–127, Apr. 1998, doi: 10.1016/S0927-0256(97)00206-1.
41. Råsander, M. (n.d.). A Theoretical Perspective on the Chemical Bonding and Structure of Transition Metal Carbides and Multilayers. https://www.researchgate.net/publication/241685137
42. Roknuzzaman, M., Ostrikov, K. K., Wang, H., Du, A., and Tesfamichael, T. (2017). Towards lead-free perovskite photovoltaics and optoelectronics by ab-initio simulations. Scientific Reports, 7(1), 1–8. https://doi.org/10.1038/s41598-017-13172-y.
43. Saikia, D., Alam, M., Bera, J., Betal, A., Gandhi, A. N., and Sahu, S. (n.d.). A First-principles study on ABBr3 (A = Cs, Rb, K, Na; B = Ge, Sn) hal ide perovskites for photovoltaic applications.
44. Setyawan, W., and Curtarolo, S. (2010). High-throughput electronic band structure calculations: Challenges and tools. Computational Materials Science, 49(2), 299–312. https://doi.org/10.1016/j.commatsci.2010.05.010.
45. Schrödinger, E. (1926). An undulatory theory of the mechanics of atoms and molecules. Physical Review, 28(6), 1049–1070. https://doi.org/10.1103/PhysRev.28.1049
46. Seitsonen, A. P. (2009). Density functional theory in the solid state. 1(2009), 20–84.
47. Shockley, W., and Queisser, H. J. (1961). Detailed balance limit of efficiency of p-n junction solar cells. Journal of Applied Physics, 32(3), 510–519. https://doi.org/10.1063/1.1736034.

48. Sholl, D. S., and Steckel, J. A. (n.d.). DENSITY FUNCTIONAL THEORY A Practical Introduction.
49. SMITH, R. C. (1975). Device Applications of the Ternary Semiconducting Compounds. Le Journal de Physique Colloques, 36(C3), C3-89-C3-99. https://doi.org/10.1051/jphyscol:1975318
50. Sreeparvathy, P. C., Kanchana, V., and Vaitheeswaran, G. (2016). Thermoelectric properties of zinc based pnictide semiconductors. Journal of Applied Physics, 119(8), 3–12. https://doi.org/10.1063/1.4942011
51. Talirz, L., Kumbhar, S., Passaro, E., Yakutovich, A. v., Granata, V., Gargiulo, F., Borelli, M., Uhrin, M., Huber, S. P., Zoupanos, S., Adorf, C. S., Andersen, C. W., Schütt, O., Pignedoli, C. A., Passerone, D., VandeVondele, J., Schulthess, T. C., Smit, B., Pizzi, G., & Marzari, N. (2020). Materials Cloud, a platform for open computational science. Scientific Data 2020 7:1, 7(1), 1–12. https://doi.org/10.1038/s41597-020-00637-5.
52. Toffoli, H. (2012). Lecture 06 : The Hohenberg-Kohn theorem and the Kohn-Sham equations. Principles of Density Functional Theory, 1964(6), 1–8.
53. Toulouse, J. (2019). Introduction to density-functional theory. 1–58.
54. Tyuterev, V. G., and Vast, N. (2006). Murnaghan's equation of state for the electronic ground state energy. Computational Materials Science, 38(2), 350–353. https://doi.org/10.1016/j.commatsci.2005.08.012
55. Widyastuti, E., Hsu, J. L., and Lee, Y. C. (2022). Insight on Photocatalytic and Photoinduced Antimicrobial Properties of ZnO Thin Films Deposited by HiPIMS through Thermal Oxidation. Nanomaterials, 12(3), 2–36. https://doi.org/10.3390/nano12030463
56. Y. Zhao and D. G. Truhlar, "Construction of a generalized gradient approximation by restoring the density-gradient expansion and enforcing a tight Lieb–Oxford bound," J Chem Phys, vol. 128, no. 18, May 2008, doi: 10.1063/1.2912068.
57. Zeb, A., Abid, M., Zeb, M. A., Qureshi, M. O., Younas, U., and Batool, I. (2020). Measurement and prediction of thermal conducti
58. vity of volcanic basalt rocks from Warsak area. Advances in Materials Science and Engineering, 2020(1), 5–12. https://doi.org/10.1155/2020/4756806
59. Zerfass, L. (2015). The ABCs of DFEs. Flexo, 40(2), 22–24
60. Zunger, A., and Wei, S. (1996). Electronic structure theory of chalcopyrite alloys, interfaces, and ordered vacancy compounds. 155(1), 84–136. https://doi.org/10.1063/1.49433